REVIEW

Hierarchical Nanostructures

ADVANCED
ENERGY
MATERIALS

www.advenergymat.de

Hierarchical Nanostructures: Design for Sustainable Water Splitting

Ming Fang, Guofa Dong, Renjie Wei, and Johnny C. Ho*

Clean and sustainable hydrogen generation renders a magnificent prospect to fulfill the humans' dream of rebuilding energy supplying systems that work eternally and run without pollution. Water electrolysis driven by a renewable resource of energy, such as wind and solar, is a promising pathway to achieve this goal, which requires highly active and cost-effective electrode materials to be developed. In this comprehensive review, we introduce the utilization of hierarchical nanostructures in electrocatalytic and photoelectrochemical applications. The unique emphasis is given on the synthetic strategies of attaining these hierarchical structures as well as to demonstrate their corresponding mechanisms for performance improvement. Rather than simply discussing all the methods that can be used in nanofabrication, we focus on extracting the rules for structural design based on highly accessible and reliable methods. Examples are given to illustrate the versatility of these methods in the synthesis and manipulation of hierarchical nanostructures, which are concentrated on nonprecious transition metals or their alloys/compounds. Through this study, we aim to establish valuable guidelines and provide further insights for researchers to facilitate their design of more efficient water splitting systems in the future.

the Earth yearly is already ten thousand times of the energy that we consume on this planet.[1,2] At present, this solar energy can be converted into electricity by using photovoltaic cells which are commercial available today; however, this solar-to-electricity conversion is facing a major challenge of its substantial costs in both materials and associated processing. Moreover, due to the intermittent nature of solar energy, it is difficult to store or distribute the obtained electricity over long distances in a low-cost manner. In this case, conversion and storage of solar energy in the form of a chemical fuel would provide a better approach to enable the more efficient energy utilizations. Hydrogen is an ideal candidate as it can be effectively produced through the scheme of water electrolysis as shown in Equation (1), in which the solar generated photovoltage is utilized to drive this reaction.[2]

$$H_2O(l) \rightarrow \frac{1}{2}O_2(g) + H_2(g) \qquad (1)$$
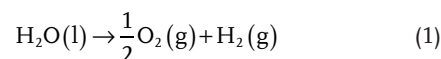
1. Introduction

Fossil fuels, the energy basis which makes our modern life possible, is depleting with an accelerated rate in recent decades resulting from the growing world population and expanding industrialization. At the same time, it is known that utilization of these traditional fuels causes emission of CO_2 as well as other hazard gases or airborne particles, which leads to severe environmental problems. Thus, developing clean and renewable alternatives to fossil fuels is crucial for the sustainability in the near future. Among many options, the solar radiation provides a clean, abundant, and renewable source of energy, and more importantly, the energy of sunlight striking onto

Following this approach, clean electrical energy can be regenerated by fuel cells when it is needed, where the hydrogen oxidation and oxygen reduction reactions convert chemical energy into electrical energy.[3,4] As compared with the method of producing hydrogen by steam reforming of fossil fuels, the solar-driven water splitting technique, which only employs water and sunlight as the source material and energy input, is obviously green and sustainable. In specific, there are several ways to facilitate reaction (1), including the configuration of photovoltaic cell plus electrolyzer, the photoelectrochemical cells (PECs) and suspended photocatalysts.[5] Among them, the PEC approach is the most economical because of its reduced

Dr. M. Fang, Dr. G. Dong, R. Wei, Prof. J. C. Ho
Department of Physics and Materials Science
City University of Hong Kong
83 Tat Chee Avenue, Kowloon, Hong Kong
E-mail: johnnyho@cityu.edu.hk

Dr. M. Fang, R. Wei, Prof. J. C. Ho
Shenzhen Research Institute
City University of Hong Kong
Shenzhen 518057, P. R. China

Dr. G. Dong
Key Laboratory of Design and Assembly of Functional Nanostructures
Fujian Institute of Research on the Structure of Matter
Chinese Academy of Sciences
Fuzhou 350108, P. R. China

Prof. J. C. Ho
State Key Laboratory of Millimeter Waves
City University of Hong Kong
83 Tat Chee Avenue, Kowloon, Hong Kong

**ADVANCED
SCIENCE NEWS**
www.advancedsciencenews.com

**ADVANCED
ENERGY
MATERIALS**
www.advenergymat.de

fabrication cost as contrasted to the first scheme and the more efficient energy harvesting by combining two different semiconductors to absorb a greater fraction of energy in the solar spectrum.

Generally, the water splitting reaction consists of two half reactions, known as the hydrogen evolution reaction (HER) and oxygen evolution reaction (OER), as described in Equation (2) and (3), respectively.

$$\text{HER:} \quad 4e^- + 4H^+(aq) \rightarrow 2H_2(g) \tag{2}$$

$$\text{OER:} \quad 2H_2O(l) \rightarrow 4H^+(aq) + 4O_2(g) \tag{3}$$
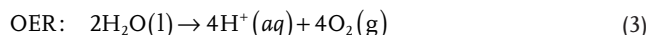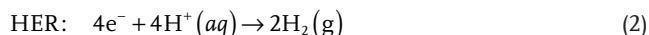
Under the standard condition, the change in free energy (ΔG) of the water splitting reaction is 237.2 kJ mol^{-1}, corresponding to an electrolysis cell voltage of 1.23 V. Nevertheless, in practice, a larger voltage is required due to the kinetic barriers occurring at both the HER and the OER sides. The overpotentials can be minimized by decorating the electrode surfaces with precious metal-based catalytic materials, for instance, Pt or IrO$_2$ for the HER and OER, accordingly;[6,7] however, the scarcities and high prices of these materials may hinder their larger scale applications. Therefore, it is of great importance to develop highly active earth-abundant catalysts to facilitate the implementation of sustainable hydrogen production. While in the PEC water splitting, semiconductors are brought into contact with water, and sunlight illuminaton is then applied to generate electron-hole pairs which can contribute to the electrolysis of water. In this case, these semiconductors are the core components of such devices, and their capacities for light harvesting and charge carrier separation are critical to the performance of PEC devices.

In principle, in both electrochemical and PEC water splitting, a large electrode–electrolyte contact area would be beneficial for the performance improvement by exposing more active catalytic sites of the electrocatalysts and increasing the areal density of photo-generated carriers at the electrode–electrolyte interface to participate the water splitting reaction in PEC systems.[8] Indeed, in recent years, scientists all over the world specialized in this particular research area have devoted huge research efforts in fabricating nanostructured materials for water splitting applications. Yet, reducing the size of a material does not necessarily infer the enhancement of its catalytic performance since the charger carrier conduction pathway has sometimes been cut off. The introduction of hierarchical 3D nanostructures would provide a better choice as it can offer an extremely high surface area while maintaining an interconnected network to ensure the excellent charge carrier conduction.[8–11]

In this review paper, we will evaluate the design and synthesis of hierarchical nanostructures targeted at their applications in the sustainable electrolytic and PEC water splitting. With this purpose, we will put emphasis on the concepts and strategies of how to design and synthesize a hierarchical nanostructure, rather than giving comprehensive comparisons of activities among different materials or listing all the methods that have been ever used. We believe that these strategies can provide valuable guidelines and further insights for researchers

Johnny C. Ho received his B.S. with high honors in Chemical Engineering in 2002, and M.S. and Ph.D. in Materials Science and Engineering from the University of California, Berkeley, in 2005 and 2009, respectively. From 2009 to 2010, he worked in the nanoscale synthesis and characterization group at Lawrence Livermore National Laboratory, California. Currently, he is an Associate Professor of Physics and Materials Science at the City University of Hong Kong. His research interests focus on the synthesis, characterization, integration and device applications of nanoscale materials for various technological applications, including nanoelectronics, sensors and energy harvesting.

to facilitate their future work in fabricating high-performance materials and devices for water splitting applications.

2. Basic Principles of Water Splitting

2.1. The HER Reaction

The HER (Equation (2)) is a two-electron transfer process with one catalytic intermediate, H* (where * denotes a site on the electrode surface), which occurs via two individual steps through either the Volmer–Heyrovsky or the Volmer–Tafel mechanism, as shown in **Figure 1**a.[12] The proton discharging, also identified as the Volmer reaction (H$^+$ + e$^-$ → H*), is the general first step which forms the absorbed hydrogen intermediate, H* on the electrode surface. Subsequently, molecular H$_2$ can be yielded via two different reaction pathways, depending on the coverage of H*. If the surface coverage of H* is low, the single H* atom would preferably join with a proton and an electron simultaneously to produce a molecule of H$_2$, known as the Heyrovsky reaction (H* + H$^+$ + e$^-$ → H$_2$). In the case of high surface coverage of H*, two adjacent H* will recombine with each other on the electrode surface to give molecular H$_2$ (2H* → H$_2$), which is recognized as the Tafel reaction. The free energy of hydrogen adsorption (ΔG_{H*}) is widely accepted as a descriptor for the hydrogen-evolving catalyst. A negative ΔG_{H*} means that the H* binds favorably with the electrode surface, which makes the initial Volmer step easy; however, if the absolute value of this ΔG_{H*} is too large, the subsequent Tafel or Heyrovsky step would be difficult. On the contrary, if a catalyst has a large and positive ΔG_H the entire reaction slow or inefficient since the interactions between protons and the electrode surface are weak. Therefore, an active HER catalyst should have a ΔG_H approaching nearly zero. Plotting this activity as a function of ΔG_{H*} can give rise to a volcano plot (Figure 1b).[13] In the plot, noble metals (e.g., Pt) have the value of ΔG_{H*} close to zero and thus exhibits the highest HER activity. Interestingly, by forming alloys of two non-noble metals from the two branches of the volcano curve, it is possible
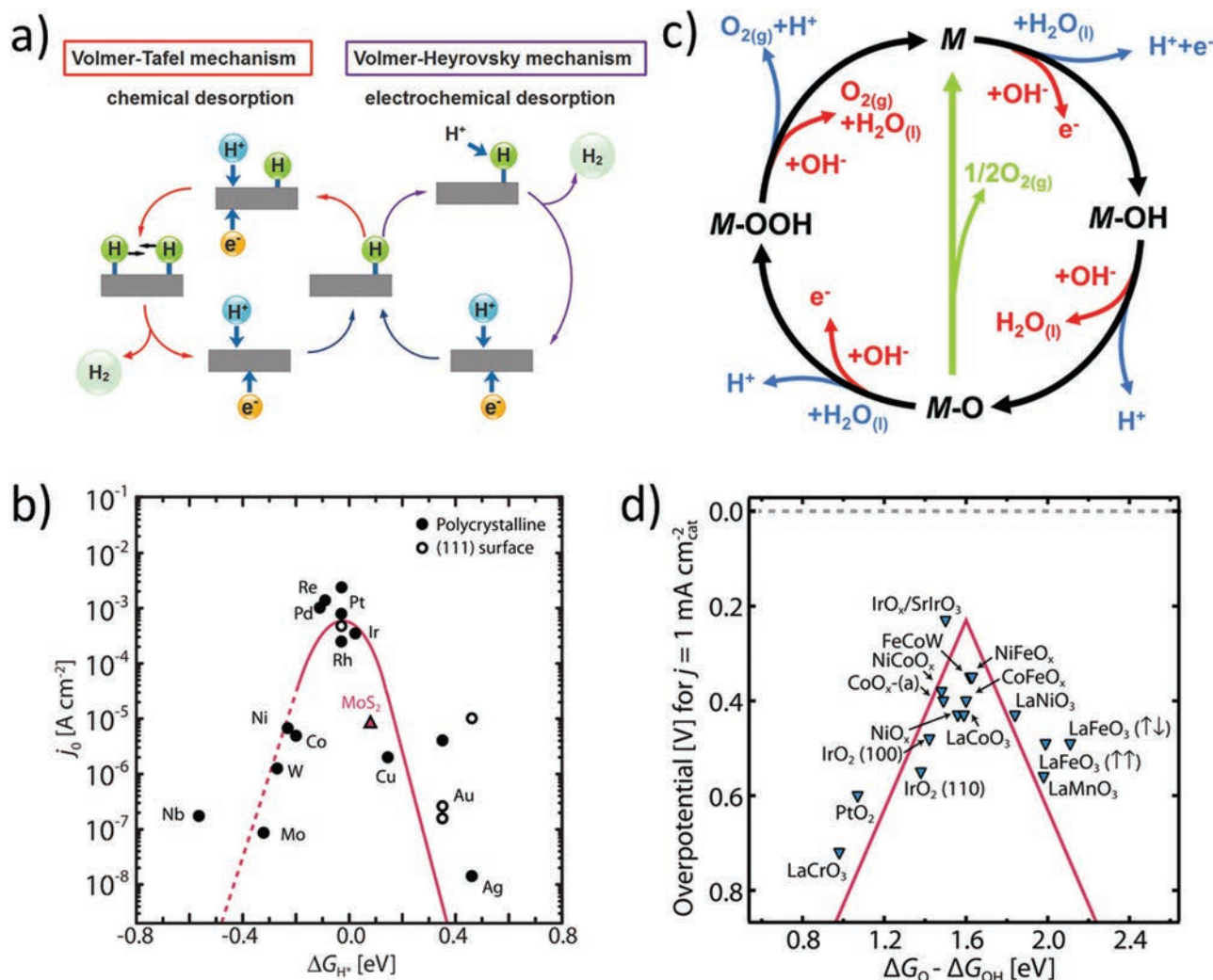
**ADVANCED
SCIENCE NEWS**
www.advancedsciencenews.com

**ADVANCED
ENERGY
MATERIALS**
www.advenergymat.de

Figure 1. a) The mechanism of HER on the surface of an electrode in acidic solution. Reproduced with permission.[12] Copyright 2014, Royal Society of Chemistry. b) HER volcano plot for metals and MoS$_2$. Reproduced with permission.[13] Copyright 2017, American Association for the Advancement of Science. c) The mechanism of OER on an electrode surface. The blue and red lines describe the reaction routes in acid and alkaline conditions. Reproduced with permission.[49] Copyright 2017, Royal Society of Chemistry. d) OER volcano plot for metal oxides. Reproduced with permission.[13] Copyright 2017, American Association for the Advancement of Science.

to obtain catalysts with enhanced catalytic performances for HER.[14–18] For example, bimetallic nickel-molybdenum (NiMo) nanowires supported on nickel foams are capable to deliver current densities as comparable to those of the state-of-the-art Pt/C catalyst.[18] However, these metal-based non-precious catalysts are not suitable for applications in acidic conditions due to their poor stability. Lately, a class of low-cost materials that combines the non-precious transition metals, such as Mo, W, Ni, Co and Fe, with nonmetal elements, including sulfur, selenium, phosphorus, nitrogen, and carbon, have attracted huge research attentions owing to their superior activity and stability for HER in a wide range of pH.[11,19–48]

2.2. The OER Reaction

The OER is a four electron–proton coupled reaction, which involves several surface-adsorbed intermediates. The OER

pathways can be occurred with different routes depending on the reaction media (i.e., acidic versus alkaline) and the specific catalyst used, but all of them involve adsorption/desorption of the oxo, peroxide and superoxide intermediates. Suen et al. have compiled the possible pathways in both acid and alkaline conditions, and summarized them in a circular flow (Figure 1c).[49] The circular flow shows that an oxygen molecule can be produced from O* intermediates either by the direct combination of two O* or through the formation and their subsequent decomposition of HOO* intermediates. The free energy change (ΔG) of OER required is 4.92 eV, and a thermochemically ideal OER catalyst is considered to have the same free energy (ΔG) for each step of the formation of (HO*, O* HOO*, and O$_2$, respectively) that equals to 1.23 eV (4.92 eV/4 = 1.23 eV) at standard conditions. This way, when a potential of 1.23 V is applied, the OER reaction would occur.[50] In any case, practically, when some of the reaction steps become downhill, some

**ADVANCED
SCIENCE NEWS**
www.advancedsciencenews.com

**ADVANCED
ENERGY
MATERIALS**
www.advenergymat.de

others remain uphill in the energy diagram, and the one having the largest ΔG would become the potential-determining step. Upon studies on a broad classes of metal oxide materials, it has been found that the binding energy of HOO* and HO* obeys a scaling relation of ($\Delta G_{HOO*} - \Delta G_{HO*} = 3.2 \pm 0.2$ eV), which means that the potential-determining step has a free energy change larger than 1.6 ± 0.1 eV and it should lie in formation processes of (HO* to O*) or (O* to HOO*). Therefore, it is possible to build a volcano curve involving the oxide based OER catalysts, by using ($\Delta G_{O*} - \Delta G_{HO*}$) as the descriptor because it is related in an expression of ($\Delta G_{O*} - \Delta G_{HOO*} = 3.2$ eV − ($\Delta G_{O*} - \Delta G_{HO*}$)).[50] Experimental results of overpotentials at 1 mA cm^{-2} of various oxide based OER catalysts are found to overlay well on the theoretical overpotential volcano curve (Figure 1d).[13,50] It is noteworthy that existence of the constant difference (i.e., 3.2 eV) between the adsorption energies of HO* and HOO* also defines a minimum overpotential of 0.4–0.2 V for the OER,[15] Therefore, the OER is intrinsically more sluggish than the HER. As it can be seen in the OER volcano curve in Figure 1d, many non-precious metal oxide based catalysts, such as nickel oxide, cobalt oxides, and their compounds with other metal oxide, can exhibit excellent OER activities, making them competitive alternatives to the precious metal-based catalysts.[51–56] In addition, some transition metal-based compounds, including chalcogenides and phosphide, display even better OER activities than the ones of oxides.[57–65] Under OER conditions, these compounds are prone to be electrochemically oxidized in the electrolyte, and the enhanced catalytic activity may be ascribed to the in situ formation of active oxide-based phases which have more exposed catalytic sites.[62,65] In some cases, the oxidization is only occurred at the surface layer, leaving a core of the starting material which can serve as electron conduction paths to improve the overall catalytic activity.[63]

2.3. Solar-Driven Water Splitting

Since the first demonstration of photo-assisted electrochemical water oxidation on an n-type TiO$_2$ electrode by Honda and Fujishima in early 1970s,[66] photocatalytic and photoelectrochemical (PEC) water splitting by using semiconducting materials have been extensively studied. To achieve photocatalytic water splitting using a single semiconductor material, its band gap must straddle the standard reduction potentials of H$^+$ and the oxidization potentials of H$_2$O, which corresponds to a bandgap value of at least 1.23 eV. In reality, due to the sluggish kinetics in water splitting, the energy required for photoelectrolysis is typically lie in the range of 1.7–2.4 eV.[9] When a semiconductor electrode is immersed into an electrolyte solution, the charger transfer would take place at the interface between the semiconductor and the redox to form an equilibrated Fermi level, causing band bending in the semiconductor and forming Schottky-type electronic junction, as illustrated in **Figure 2**. This junction can be utilized for the charge carrier separation. For a n-type semiconductor that have the top of the valence band being more positive than the oxidation potential of H$_2$O/O$_2$, photoexcited holes would drift to the semiconductor surface by the internal electric field due to band bending, and hence, the semiconductor can act as a photoanode to oxidize water (Figure 2a). Similarly, a p-type semiconductor can function as a photocathode for the hydrogen evolution given that the bottom of its conduction band is more negative than the proton reduction potential (Figure 2b). A tandem PEC cell may be constructed when a photoanode is connected to a photocathode, which ultimately allows full water splitting by integrating various small bandgap semiconductors (Figure 2c).

3. Hierarchical Nanostructures and their Applications in Water Splitting

3.1. Definition of Hierarchical Nanostructures

Usually, a hierarchical nanostructure is an integrated architecture composed of nanoscale or low dimensional subunits, including zero dimensional (0D) nanoparticles, one dimensional (1D) nanowires or nanotubes, and two
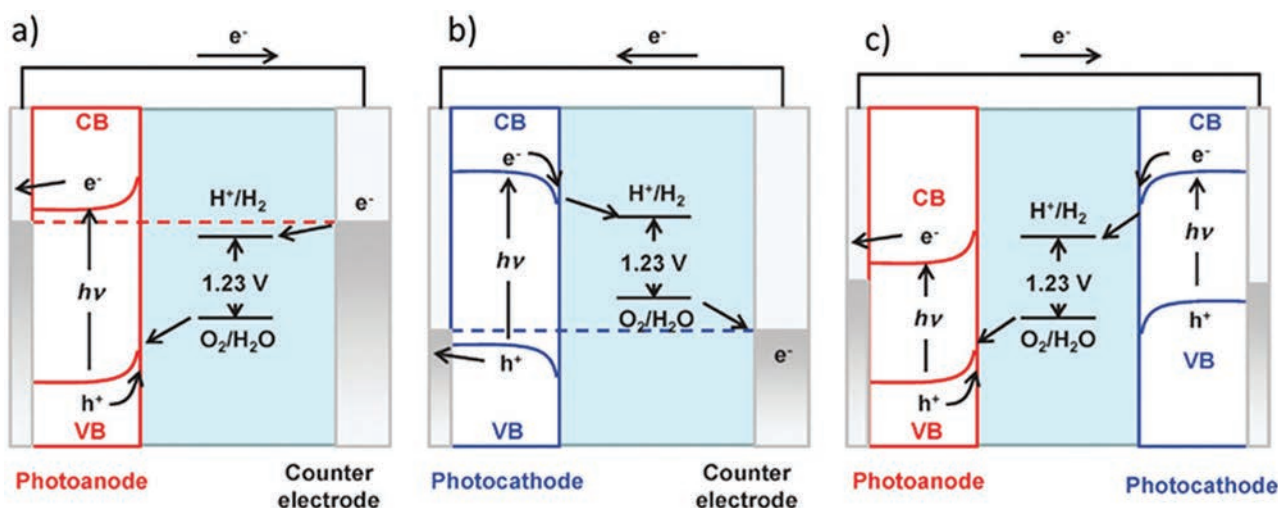

Figure 2. Energy band diagrams of a PEC cell for water splitting by using a) a photoanode, b) photocathode, and c) photoanode and photocathode in tandem configuration. Reproduced with permission.[67] Copyright 2014, Royal Society of Chemistry.

**ADVANCED
SCIENCE NEWS**

www.advancedsciencenews.com

**ADVANCED
ENERGY
MATERIALS**

www.advenergymat.de

dimensional (2D) nanosheets, in which these sub-units are characteristically aligned in a well ordered fashion.[10] In fact, hierarchical structures are always observed in nature, such as the trees which have trunks and branches, flowers made of petals, and the sea urchins having arrays of needles on the surface. When these structures are mimicked and fabricated in nanoscale configurations, the physical properties of those original materials can be modulated widely and precisely, providing wonderful opportunities to improve their performance for many different technological applications.

3.2. Hierarchical Nanostructures for Electrochemical Water Splitting

To obtain a high mass activity of an electrocatalyst, it is essential to make the material small enough so that the improved surface to volume ratio would facilitate more active sites being exposed to the electrolyte to participate in the reaction. However, at the same time, this size reduction also brings along adverse effects for the performance improvement, for instance the increased charge transfer resistance. In this case, fabricating the catalyst into hierarchical nanostructures can effectively avoid these problems by providing seamless contact to the sub-units. Simultaneously, the utilization of hierarchical nanostructures can offer many other advantages, such as enhancing the electrolyte penetration, accelerating the bubble release rate by providing the larger free space, and avoiding the random particle aggregation. There has been a huge amount of reports demonstrating all these above-mentioned advantageous effects of using hierarchical nanostructures as the catalyst for electrochemical water splitting. Essentially, the most active nonprecious HER and OER catalysts reported so far all have the hierarchical structures. For instance, Tang et al[48] have fabricated self-standing $Fe_xCo_{1-x}P$ ternary nanowire arrays on carbon clothes ($Fe_xCo_{1-x}P$ /CC), which possess the Pt-like activity for HER with the need of overpotential of only 37 mV to drive 10 mA cm^{-2} in 0.5 M H_2SO_4. For water oxidation, Xu et al[68] have developed $Ni_xFe_{1-x}Se_2$-derived OER catalysts supported on nickel foams that require an overpotential of only 195 mV for 10 mA cm^{-2}.

3.3. Hierarchical Nanostructures for PEC Water Splitting

For PEC water splitting, hierarchical nanostructures are also helpful for the performance improvement possibly through: 1) increasing the light harvesting by the minimization of optical reflection due to the graded effective refractive index; 2) improving the charge carrier collection efficiency by the reduction of total thickness of the semiconductor; 3) accelerating the charge transfer by the creation of large surface area to contact with electrolyte which will cause band bending within the semiconductor; 4) enabling the design of heterojunctions by the introduction of a second semiconductor material; and 5) providing enough space for the catalyst loading.[5,69–71]

4. Strategies for Fabricating Hierarchical Electrocatalysts

4.1. General Approaches for the Synthesis of Transition Metal Based Nanomaterials

As discussed in the previous section, for the efficient water splitting, highly active and cost-effective catalysts should be developed to replace the precious metal based catalysts for both HER and OER processes. According to the recent progress, highly accessible transition metal based alloys or compounds could be employed as the effective alternatives. Among them, iron group transition metal oxides and hydroxides are highly active catalysts for OER. Transition metal alloys, chalcogenides, phosphides, carbides, nitrides, and borides have been considered as the highly active catalyst for HER in wide pH ranges, and some of them, such as NiP, CoP and CoSe, can also function as the highly efficient bifunctional catalysts for both HER and OER in alkaline conditions. It can be envisioned that by combining with numerical computing, increasingly more catalysts based on these above-discussed elements will be discovered and further explored. Therefore, it is necessary to generalize the present synthetic methods for guiding the design of catalyst that would emerge in the future. **Figure 3**a shows a diagram of general strategies for the synthesis of various transition metal based materials by taking a chemistry
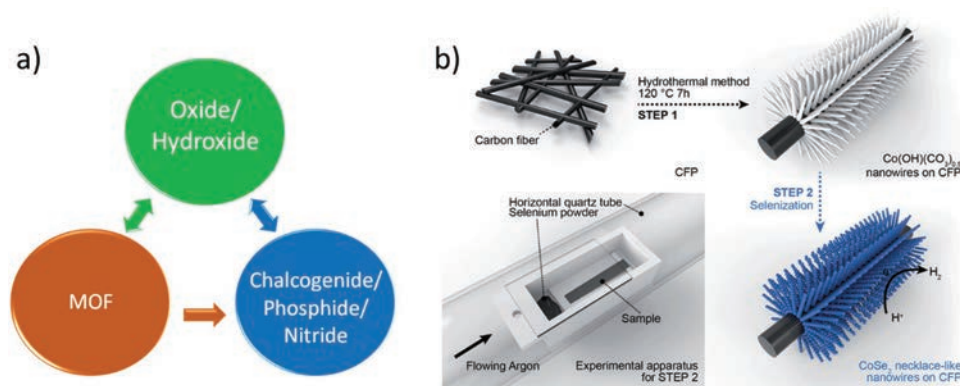

Figure 3. a) General strategies for the synthesis of transition metal based nanomaterials by precursor conversion. b) An example shows the fabrication of necklace-like CoSe$_2$ nanowires arrays on carbon fibers by first hydrothermal synthesis of Co(OH)(CO$_3$)$_{0.5}$ nanowire precursors and followed thermal treatment under Se vapor. Reproduced with permission.[30] Copyright 2015, Royal Society of Chemistry.

**ADVANCED
SCIENCE NEWS**
www.advancedsciencenews.com

**ADVANCED
ENERGY
MATERIALS**
www.advenergymat.de

viewpoint. In principle, it is possible to achieve templated synthesis of a specific materials (e.g., metal sulfide) by the direct or indirect chemical conversion from other the forms (e.g., metal hydroxide or MOF). Many methods, such as thermal conversion and ion exchange reaction, can be utilized to transform these transition metal-based compounds into desired chemical compositions for catalytic applications. For example, metal oxide/hydroxide can be converted into sulfide, selenide, phosphide by thermal treatment under S, Se and P vapors in inert conditions, respectively; while thermal or electrochemical oxidization of the latter compounds allows the formation of metal oxide materials. Figure 3b depicts an example of the synthesis of $CoSe_2$ nanowires on carbon fibers by the thermal treatment of hydrothermally synthesized $Co(OH)(CO_3)_{0.5}$ nanowires under Se vapor. Although the morphology has been changed during the fabrication process, majority of the wire-like features has been well-preserved.

4.2. Hydrothermal Synthesis

4.2.1. Introduction of Hydrothermal Synthesis

The hydrothermal method is one of the most popular approaches in the nanomaterial synthesis due to its simplicity and flexibility in morphology control. Generally, the hydrothermal synthesis involves heterogeneous chemical reactions in aqueous media in autoclaves at a temperature higher than room temperatures, normally exceeding 100 °C, under pressure levels higher than 1 atm.[72] Under hydrothermal conditions,

the unusual reaction may occur and the reaction rate may be accelerated, which allows the formation of crystalline materials at relative low temperatures. Several factors, including the precursor concentration, temperature, reaction time, complex agents, and the solution pH, can affect the nucleation and growth of the crystals, and therefore, it is possible to manipulate the morphology by controlling these factors.[73–77] Similarly, organic solvents can as well be used to dissolve the precursors, and this synthesizing technique is known as the solvothermal synthesis. Nevertheless, in many instances, "hydrothermal" has been used with a broader meaning that covers both cases.[10]

4.2.2. Self-Organized Nanostructures Supported Hierarchical Nanostructures

In the hydrothermal synthesis, due to the presence of water, the reactants can move freely in the solution, hierarchical architectures can then be preferentially formed without using any external template. This way, a wide range of transition metal-based hierarchical nanomaterials have been synthesized by these hydrothermal approaches. **Figure 4** displays scanning electron microscope/transmission electron microscope (SEM/TEM) images of self-organized hierarchical nanostructures prepared by hydrothermal/solvothermal reactions, including α-$Ni(OH)_2$,[78] Co_3O_4,[79] $WO_{2.72}$,[80] $NiCo_2O_4$,[81] $Ni_{0.85}Se$[82] and MoS_2.[83] All of these materials can be directly used as catalysts, or as precursors of catalysts for applications in HER or OER. For instance, hierarchical nanostructured α-$Ni(OH)_2$ catalysts prepared by the hydrothermal reaction can be afforded with
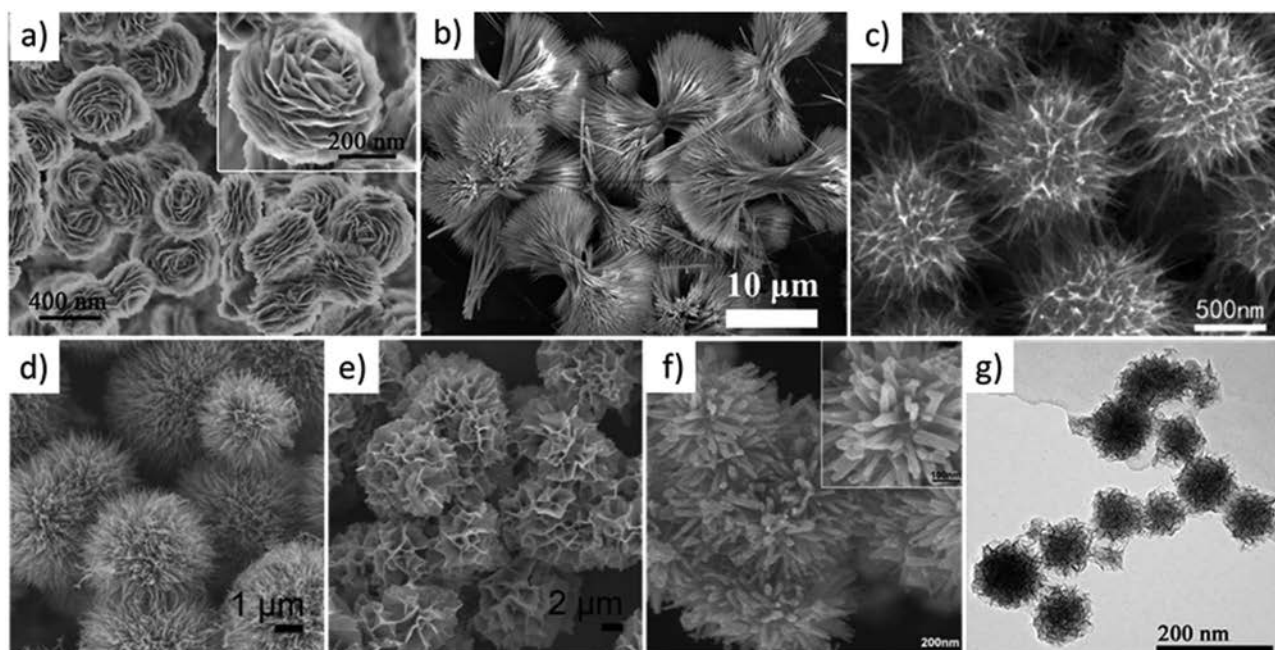

Figure 4. Self-organized hierarchical nanostructures by hydrothermal/solvothermal synthesis. a) SEM image of α-$Ni(OH)_2$ nanoflowers. Reproduced with permission.[78] Copyright 2014, Royal Society of Chemistry. b) SEM image of Pompon-like Co_3O_4 porous structures. Reproduced with permission.[79] Copyright 2014, Royal Society of Chemistry. c) Urchin-like $WO_{2.72}$ nanostructures. Reproduced with permission.[80] Copyright 2012, American Chemical Society. d,e) Morphology-controlled $NiCo_2O_4$ hierarchical nanostructures. Reproduced with permission.[81] Copyright 2013, Royal Society of Chemistry. f) Urchin-like $Ni_{0.85}Se$ nanostructures. Reproduced with permission.[82] Copyright 2007, Elsevier Ltd. g) TEM of image of self-organized MoS_2 nanospheres. Reproduced with permission.[83] Copyright 2015, Nature Publishing Group.

ADVANCED
SCIENCE NEWS
www.advancedsciencenews.com

ADVANCED
ENERGY
MATERIALS
www.advenergymat.de

an OER current density of 10 mA cm^{-2} at a small overpotential of 0.331 V and a small Tafel slope of ≈42 mV/decade, which is comparable to the state-of-the-art RuO$_2$ catalyst.[84] Also, the CoP nanostructures converted from urchin-like cobalt carbonate hydroxide precursors can exhibit a low HER onset overpotential of 50 mV, a small Tafel slope of 46 mV dec^{-1}, and a low overpotential of ≈180 mV at a current density of 100 mA cm^{-2} in 0.5 M H$_2$SO$_4$.[85]

The formation of hierarchical nanostructure may be proceeded with the following steps: i) nucleation, ii) nuclei aggregation under the driving forces of high surface energy and electrostatic interactions, iii) nanocrystal formation from aggregated nuclei to further lower the surface energy, iv) anisotropic growth of the crystal along a preferred crystal axis seeded from the nanocrystals due to the lower energy barrier, and v) further growth by Ostwald ripening, during which unstable smaller particles dissolve and larger particles grow by adsorbing monomers from the dissolved particles driven by the surface energy minimization.[86] While under some circumstances, especially in the systems where co-solvents or complexing agents exist, the growth would follow different pathways. For example, the hydrothermal growths of carnations-like Ni(OH)$_2$ (Figure 4a) and Co(OH)$_2$ nanoflowers in water–ethylene mixtures have been found to proceed via the formation of separate Co(OH)$_2$ nanosheets and followed by the layer-by-layer assembly of these nanosheets.[78,87] Other mechanisms, such as the crystal splitting mechanism, have also been found to play important roles in the synthesis of urchin-like architectures.[79,88]

4.2.3. Support/Templated Synthesis

Growth of nanomaterials on the nanoscale substrate is a more reliable and generalizable approach to synthesize hierarchical nanomaterials. In some cases, seed layers are needed for the growth of well-ordered nanostructures on a supporting substrate. For example, nanocrystals of TiO$_2$ and ZnO are often pre-coated on a substrate before the growth of TiO$_2$ and ZnO nanorod arrays, respectively. While for many transition metal hydroxides, such as nickel and cobalt hydroxides which have strong tendencies to form instrisic anisotropic 2D crystals, uniform nanoarrays of these materials can be grown on various substrates without using seed layers. Carbon-based low dimensional nanomaterials including 1D carbon nanotubes (CNTs) and 2D graphene have been extensively utilized as templating substrates for forming various hybrid nanomaterials, due to their larger surface area, outstanding electron conductivity, and excellent chemical stability. As these carbon materials are hydrophobic, wet chemical treatment of them in oxidic acid (e.g., concentrated H$_2$SO$_4$ and HNO$_3$) are often applied before being used as substrates by introducing hydrophilic oxygen-containing functional groups on the surfaces. Growth of electrocatalysts on these functionalized CNTs and graphene would at least offer the following advantages: 1) providing nucleation sites which avoids the formation of large-sized particles and thus increases surface area of the material; 2) reducing the charge transport resistance due to their high electron conductivity. **Figure 5**a shows a typical TEM image

of MoS$_2$ nanosheets wrapped on 1D multi-wall carbon nanotubes (CNTs) synthesized by the hydrothermal reaction of (NH$_4$)$_6$Mo$_7$O$_{24}$·4H$_2$O and thiourea using oxidized CNTs as the templates.[89] It is found that under the similar condition, without CNTs, the obtained products are large MoS$_2$ aggregates. As a result, the MoS$_2$–CNT nanocomposite exhibits the remarkably improved electrocatalytic activity towards HER, which can reach a current density of ≈850 mA cm^{-2} with an overpotential of only 290 mV and maintain a low Tafel slope of 47 mV dec^{-1} even under a high current density region. Figure 5b demonstrates a representative SEM image of FeP nanowire arrays vertically supported on reduced graphene oxide (rGO) fabricated by pseudomorphoic transformation of hydrothermally synthesized FeO(OH) NWs/GO precursors.[90] Owing to the improved electrode/electrolyte interaction and the efficient utilization of the catalysts, the 3D FeP NWs/rGO electrocatalyst exhibits the enhanced HER performance and better stability than FeP NWs assemblies and FeP nanoparticles on reduced graphene oxide (NPs/rGO). In addition to nanoscale 1D and 2D substrates, conductive microporous substrates such carbon fiber papers (CFP) and nickel foam (NF) have also been frequently utilized to fabricate binder-free, monolithic and 3D hierarchical architectures for electrocatalytic applications. Figure 5c displays the SEM and TEM (inset) images of necklace-like CoSe$_2$ nanowires on woven carbon fiber papers (CFP) prepared by the hydrothermal growth on CFP and followed by the selenization at 450 °C.[30] Interestingly, the necklace-like morphology is formed after the selenization, possibly due to the fast reaction between the single-crystalline Co(OH)(CO$_3$)$_{0.5}$ NWs and the highly active selenium vapor. The CoSe$_2$ necklace-like NWs on CFP only needs modest overpotentials of 188 and 199 mV to afford the current densities of 50 and 100 mA cm^{-2} for HER in the acid electrolyte, accordingly. Similarly, by using microporous NF as the substrate, combining with the hydrothermally growth and ion exchange reaction, hierarchal architectures composed of vertically aligned CoS NW arrays and microporous NF have been achieved (Figure 5d),[91] which could also be employed as efficient electrocatalysts for water splitting reactions.

4.2.4. Summary on the Hydrothermal Method in Hierarchical Nanostructure Fabrications

Through the above examples, it can be seen that hydrothermal is a very powerful tool for synthesizing various functional nanomaterials of transition metal compounds, such as oxides, hydroxides, and sulfides. In many cases, self-organized hierarchical nanostructures, such as nanoflowers and nanourchins, can be obtained autogenously. Utilization of templates offers a more reliable way for the nanostructure design. Moreover, besides to assist the growth of the hierarchical nanostructures, the template can also be functional when the synthesized material is used as catalyst, leading to performance enhancement. Although catalyst grown on monolithic microporous conductive substrates often show very good catalytic performances, the fabrication is not economical because only a small fraction of the reaction products adhered in the
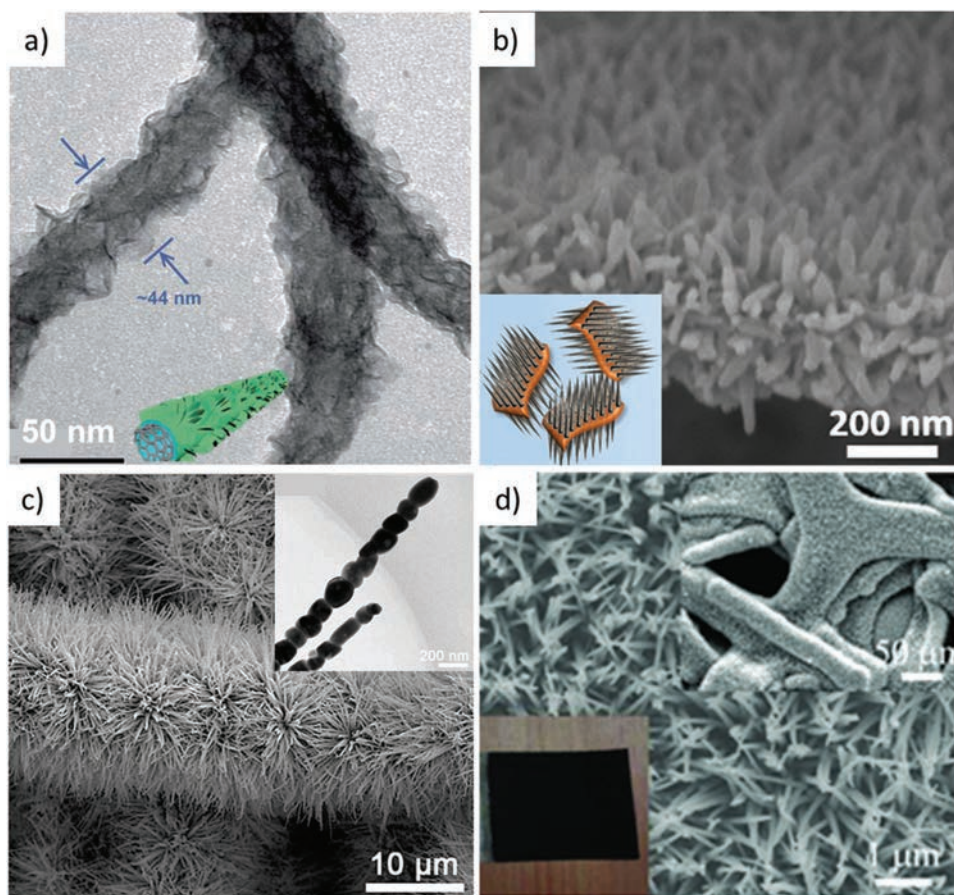
**ADVANCED
SCIENCE NEWS**
www.advancedsciencenews.com

**ADVANCED
ENERGY
MATERIALS**
www.advenergymat.de

Figure 5. Hierarchical nanostructure grown with supporting substrates. a) TEM image of MoS$_2$ nanosheets wrapping on carbon nanotubes. Reproduced with permission.[89] Copyright 2017, Royal Society of Chemistry. b) SEM image FeP nanorods supported on reduced graphene oxide. Reproduced with permission.[90] Copyright 2015, John Wiley and Sons. c) Necklace-like CoSe nanowires on woven carbon fiber paper. Reproduced with permission.[30] Copyright 2015, Royal Society of Chemistry. d) CoS nanowire arrays on microporous nickel foam. Reproduced with permission.[91] Copyright 2014, John Wiley and Sons.

substrate and the majority precipitated down to the bottom of the autoclave vail.

4.3. Electrochemical Deposition

4.3.1. General Working Principle of Electrochemical Deposition

Electrochemical deposition (ED) is a process using electricity to deposit materials from solutions on conductive substrates. A well-known technique of ED is electroplating, which uses electric current to reduce metal cations and then to form metal coatings. Metal oxide, hydroxide, sulfide, and phosphide that have potential applications as electrocatalysts, can also be synthesized by electrodeposition. Although the deposited materials are different in their chemical compositions, the working principles are quite similar. That is to generate a new species, in most cases a new kind of anions or cations that can form precipitates when encountering with other species in the solution. As the reaction is taken place locally around the electrode, depositing hierarchically structured materials are possible by using a conductive and microporous substrate, such as the

commercially available nickel foam, stainless steel meshes, and woven carbon fibers.

4.3.2. Hydrogen Bubble Dynamic Template (HBDT) Deposition

Lately, a special scheme of electroplating, which is called the hydrogen bubble dynamic template (HBDT) deposition, has attracted numerous attentions for its versatility in fabrications of hierarchical porous metal nanostructures without the use of additional templates.[92] The HBDT occurs at a relatively large cathodic potential, which enables simultaneous reductions of both the metal cations and the protons in the solution, so that H$_2$ bubbles evolved can be used as a dynamic template during the electrodeposition process. Cu has been utilized as a model material in the mechanistic studies of the nucleation and dendrite growth.[93–99] **Figure 6**a shows the illustration of bubble assembly behavior in the acidic electrolyte, and Figure 6b and c display the SEM images of hierarchical Cu nanostructures deposited by the HBDT technique.[98,99] The bubbles coalescence induces the formation of larger-sized bubble templates. Eventually, the small-sized holes are formed at the bottom and the large
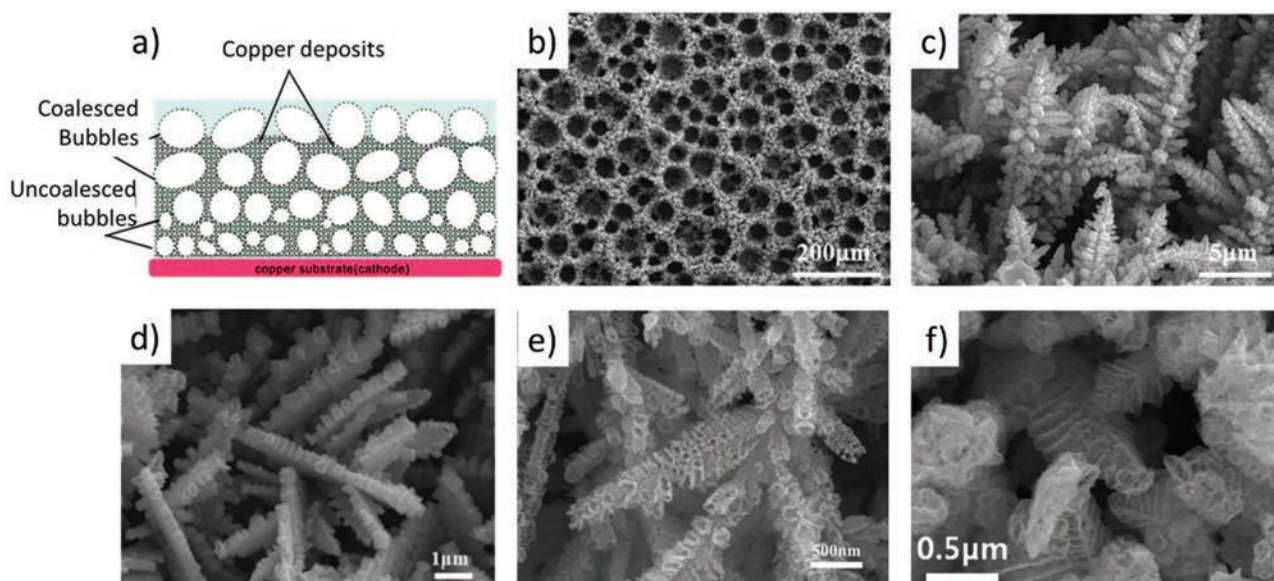
**ADVANCED
SCIENCE NEWS**

www.advancedsciencenews.com

**ADVANCED
ENERGY
MATERIALS**

www.advenergymat.de

Figure 6. Hierarchical nanostructure fabrications by hydrogen bubble dynamic template (HBDT) synthesis. a) Schematic illustration of the effect of hydrogen bubble coalescence on the formation of the honeycomb-like porous structure. Reproduced with permission.[98] Copyright 2013, The Electrochemical Society. b,c) SEM images of HBDT-deposited Cu. Reproduced with permission.[99] Copyright 2014, Royal Society of Chemistry. d) SEM images of HBDT-deposited Ni-Sn alloy. Reproduced with permission.[117] Copyright 2013, Elsevier Science Ltd. e) SEM image of hollow Ni nanostructures obtained by de-alloying a HBDT-deposited Ni-Cu alloy. Reproduced with permission.[108] Copyright 2015, Royal Society of Chemistry. f) SEM image of hollow RuO2 nanostructures after de-alloying a HBDT-deposited Ru-Cu alloy. Reproduced with permission.[113] Copyright 2013, Elsevier Science Ltd.

ones are formed later on the top. At the same time, the initiation of hydrogen bubbles on the deposit side wall would contribute to the evolution of dendritic structures. Other metals, such as Ni,[100] Co,[101] Sn,[94] Ag,[102] Au,[103] Ru,[104] Pd,[105–107] and a series of bimetallic porous nanostructures have also been prepared by the HBDT method, including Cu-Ni,[108–110] Cu-Au,[111] Cu-Pd,[112] Cu-Ag,[111] Cu-Ru,[113] Cu-Pt,[114,115] Ni-Sn,[116,117] Ni-Co,[118] Ni-Mo,[119] Ni-Ag,[120] Pt-Ag,[121] and Pt-Pd.[115] Figure 6d gives a typical SEM image of the porous $Ni_{50}Sn_{50}$ alloy with the tube-like dendritic structure, whose tube diameter is less than 100 nm and the length of dendritic branches is about 5 μm.[117] By selective leaching or de-alloying, bimetallic porous structures can be further converted into the more-porous and mono-metallic hollow structures. For instance, highly nano-porous Ni has been fabricated by Choi et al.[108] by HBDT deposition of dendritic Ni-Cu layer and then electrochemical de-alloying of the copper in a H_2SO_4 solution (Figure 6e). Nano-porous and dendritic Ru has as well been prepared by employing the similar HBDT deposition and de-alloying approach (Figure 6f).[113] Notably, through the de-alloying process, the BET (Brunauere–Emmette–Teller) surface area is found to increase from 23.5 m^2 g^{-1} (as-deposited Ru-Cu) to 207.5 m^2 g^{-1}. Moreover, the deposited 3D porous metal structures can be further transformed into noble-metal foam films of Ag,[122] Au,[103,123] Pt,[107,124,125] or Pd[122,126] via the galvanic replacement reaction that can be carried out by direct immersion of the metal deposit into solutions containing noble-metal salts.

Combining with the merits of very large surface area and excellent electron conductivity, these HBDT-obtained 3D structures hold the great potential for electrocatalytic applications. 3D Cu_2O–Cu hybrid foams have been developed as high-performance electrocatalysts for OER in the alkaline solution. The

hybrid foams are composed of Cu_2O–Cu dendrites with high surface area, high-speed electronic transport networks. While a reference Cu wire shows the very limited OER activity, the foams of Cu, CuO_2 and Cu_2O–Cu exhibit evidently the much-enhanced activities. The overpotential needed for driving a current density of 10 mA cm^{-2} for the Cu_2O–Cu foam is 60 and 37 mV less than those of Cu foams and Cu_2O foams, respectively. Importantly, the hybrid Cu_2O–Cu foam is also demonstrated with the excellent durability at a current density of 10 mA cm^{-2} over 50 h for OER in the alkaline solution.

4.3.3. Cathodic Deposition of Well-Ordered Hydroxide Nanoarrays

The electrodeposition of well-ordered first-row transition-metal (e.g., Fe, Co, and Ni, etc.) hydroxides are enabled by passing current through electrolytes containing these transition metal cations and nitrate anions (NO_3^-).[57,127–136] The process is based on the reduction of nitrate to ammonium ions, as described in Equation (4):

$$NO_3^- + 7H_2O + 8e^- \rightarrow NH_4^+ + 10\,OH^- \tag{4}$$
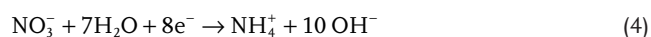
The produced hydroxide ions (OH^-) would then elevate the local pH, resulting in the precipitation of metal hydroxide at the electrode surface, for example in the case of $Ni(OH)_2$ deposition:

$$Ni^{2+} + 2OH^- \rightarrow Ni(OH)_2 \tag{5}$$

In most cases, the as-deposited transition metal hydroxides are demonstrated with the morphology of vertically aligned

nanosheets or nanowalls on the substrate, possibly due to their tendency to form layered crystalline structures. High performance hierarchical OER catalysts have been prepared by co-deposition of Ni-Fe hydroxide nanosheets on microporous substrates.[135,136] Lu et al.[135] have prepared a hierarchical Ni-Fe hydroxide/nickel foam (denoted as NiFe/NF) catalyst that only requires 215 mV to obtain a current density of 10 mA cm^{-2} in 1 M KOH while it can deliver a current density of 500 mA cm^{-2} at an overpotential of 240 mV in 10 M KOH. Almost at the same time, Li et al.[136] has fabricated a series of Fe-containing layered double hydroxides (MFe-LDHs, M = Ni, Co and Li) based hierarchical nanosheet arrays on various substrates, including nickel foam, carbon fiber cloth and FTO glass, under the cathodic potential. As depicted in **Figure 7**, among those obtained catalysts, the NiFe-LDH nanoplatelet arrays display the best catalytic performance in OER, giving a relatively low overpotential (224 mV) at 10 mA cm^{-2} in 1 M KOH,[133] much superior to the previously reported OER catalysts as well as the state-of-art Ir/C catalyst, which is also in a good consistence with the results reported by Lu et al.[135]

4.3.4. Potentiodynamic Deposition of Well-Ordered Transition Metal Sulfide Nanoarrays

The research on electrodeposited metal sulfide has been largely pushed in advance with the motivation of finding cost-effective alternatives to Pt as counter electrode materials in dye-sensitized solar cells (DSSCs).[137–143] To obtain well-ordered nanostructures, thiourea (TU) has been employed as an ion complexing agent and sulfur source.[142] As described in Equation (6) and (7), under cathodic potentials, Co(II)–TU complexes are reduced to the compounds of CoS.

$$Co^{2+} + 2TU \rightarrow Co(TU)_2^{2+} \qquad (6)$$

$$Co(TU)_2^{2+} \xrightarrow{\text{reduction}} CoS\downarrow \qquad (7)$$

Many efforts have as well been devoted to fabricate hierarchically structured metal sulfide and explore their applications in supercapacitors,[144–146] lithium ion batteries,[147] and electrocatalytic water splitting reactions.[27,148,149] It is found that the potentiodynamic deposition mode can facilitate the formation of CoS compounds as compared with the conventional chronoamperometric method, which can be attributed to the more efficient formation of Co(II)–TU complexes under the potentiodynamic condition.[142] Despite, it is also possible to achieve well-ordered nanoarrays under chronoamperometric conditions by changing the electrolyte constitutions. Wang et al. recently have designed a hierarchically integrated 3D electrode composed of carbon paper (CP), carbon nanotubes (CTs), and CoS sheets (**Figure 8**), which exhibits the high activity and stability toward both HER and OER in the alkaline medium.[149] The CoS nanosheets can be synthesized by applying a constant potential of −0.9 V vs Ag/AgCl to the CP/CTs electrode, where the electrodeposition bath is an ethanol–water solution with a volume ratio of 3:7, containing 0.1 M cobalt nitrate hexahydrate and 0.5 M thiourea.

It is noteworthy that many other transition metal chalcogenide, such as molybdenum sulfide, cobalt selenide, and nickel phosphide have likewise been synthesized by electrodeposition methods; however, these obtained materials are often come
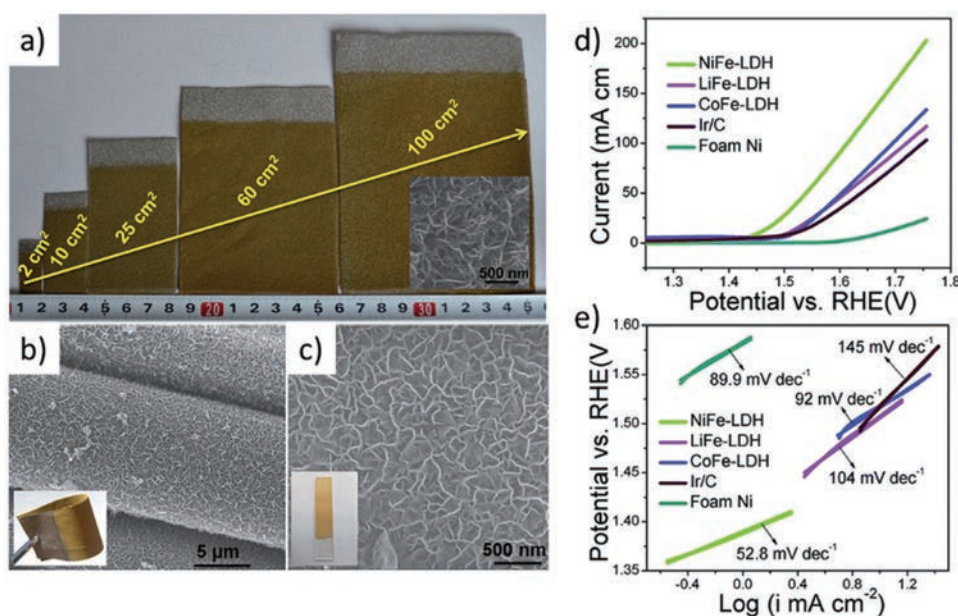

Figure 7. a) Photographs of NiFe-LDH nanoplatelet arrays synthesized on the foam nickel substrates with various scales inset: the SEM image of NiFe-LDH on 100 cm^2 substrate. b,c) SEM images for NiFe-LDH nanoplatelet arrays on carbon fiber cloth and FTO substrate, respectively (inset: their corresponding photographs). d,e) Linear sweep voltammetric (LSV) curves and Tafel plots of the cathodic deposited LDH catalysts and the commercial Ir/C catalyst. Reproduced with permission.[136] Copyright 2015, Royal Society of Chemistry.
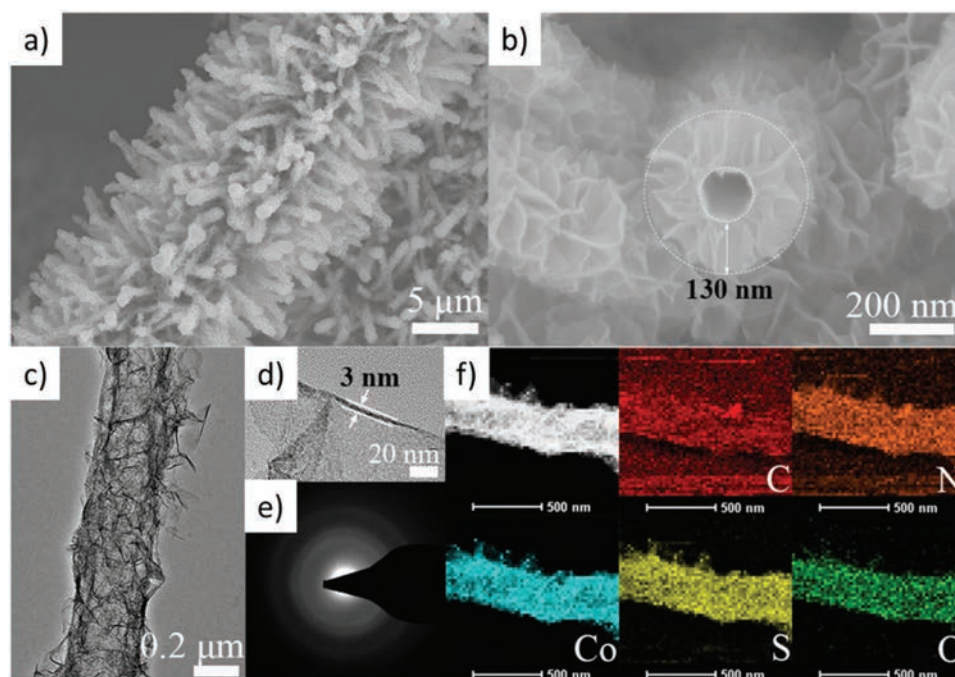
**ADVANCED
SCIENCE NEWS**

www.advancedsciencenews.com

**ADVANCED
ENERGY
MATERIALS**

www.advenergymat.de

Figure 8. a,b) SEM images of CP/CTs/Co-S. c,d) TEM images. e) SAED pattern, and f) element mapping of CT/Co-S. Reproduced with permission.[149] Copyright 2016, American Chemical Society.

with uncontrolled morphologies, which are not favorable for the design of hierarchical nanostructures.[150,151] Therefore, those corresponding fabrication methods would not be discussed in detail here.

4.3.5. Summary on the Electrodeposition Methods in Nanofabrication

Electrodeposition is often an underestimated or omitted method in nanofabrication. However, through our survey, one can find that it is actually very useful in fabrications of dendritic hierarchical structures as well as many well-ordered transition metal oxide, hydroxide, and sulfide. Also, the electrodeposition method holds some overwhelming advantages as compared with the hydrothermal method, including its excellent safety, relatively low processing temperature, high accessibility (electroplating systems have been well-established in the printed circuit board, PCB, industry), short deposition time (for deposition of nanostructure, often only need a few to tens of minutes) and minimized material waste. Nevertheless, all these do not imply the electrodeposition method being the best fabrication method. Due to the fast reaction time, the electrodeposited materials are often amorphous or having the low crystallinity, which are not favorable for certain applications.

4.4. Metal-Organic Complex/Frameworks Directed Synthesis

4.4.1. Introduction to MOF

Metal-organic frameworks (MOFs) are an emerging class of porous materials that consist of coordination bonds between transition-metal cations and organic ligands.[152] Most of the transition metal cations can be used to form MOFs-based nanostructures by using appropriate organic ligands under mild conditions.[153–155] Therefore, MOFs have been recently developed as versatile precursors for the synthesis of highly porous transition metal based nanomaterials for electrocatalytic applications.[156–158] As there have been many excellent review articles regarding the synthesis of various MOFs,[159–163] in this section, we step straightforward to the processing strategies of designing hierarchically structured electrocatalysts using well-defined MOF precursors.

4.4.2. MOF-Directly Synthesis of Transition Metal Oxides, Hydroxides, and Sulfides

The high porosity of MOFs not only makes them intriguing for their direct applications in widespread areas, but also provides huge opportunities allowing individuals to obtain well-structured porous inorganic nanomaterials which otherwise cannot be synthesized by conventional inorganic methods. Oxide-based porous nanostructures can be produced conveniently by calcination of MOF nanostructures (such as nanosheets, nanocubes, nano-octahedrons, etc.) in air, with careful control over the temperature, heating rate as well as the calcination time to avoid the structure collapse.[164–167] Alternatively, transition metal layered double hydroxide (LDH) can be obtained using certain MOF precursors, such as zeolitic imidazolate frameworks (ZIFs) being a class of metal-organic frameworks that are topologically isomorphic with zeolites. ZIFs are composed of tetrahedrally coordinated transition metal cations (e.g., Fe, Co, Cu, Zn) connected by imidazolate linkers.[168,169]

**ADVANCED
SCIENCE NEWS**

www.advancedsciencenews.com

**ADVANCED
ENERGY
MATERIALS**

www.advenergymat.de

It has been found that LDH hollow nano-polyhedra can be synthesized by simply thermal treatment of Co-based ZIF-67 nanocrystals in an ethanol solution containing $Ni(NO_3)_2$. **Figure 9**a–h display the digital, SEM and TEM images related to ZIF-67 precursors and the obtained LDH nanocages.[170] It can be seen that the nanocages consist of very thin LDH sheets and the primary polyhedral morphology is well preserved. The formation of the LDH is triggered by the hydrolysis of the $Ni(NO)_2$ in the ethanol solution because this chemical process increases the solution acidity and causes the release of Co^{3+} from the ZIF. The slowly released Co^{3+} ions then co-precipitate with Ni^{2+} to form LDH. Through this mechanism, LDH

nanocages with different compositions, including Mg-Co, Ni-Co and Co-Co LDH, have been synthesized.[171] Interestingly, the reaction from ZIF to oxide/hydroxide can be reversed, which allows the templated synthesis of MOFs nanostructures. For example, as shown in Figure 9i, the zinc nitrate hydroxide nanosheets can be converted to ZIF-8 (zinc-containing ZIF) by immersing them in a 2-methylimidazole solution, and the ZIF-8 can be transformed back into LDH in $Ni(NO_3)_2$ or $Co(NO_3)_2$ solutions.[172] Moreover, the Zn component can be removed from the LDH in alkaline solutions, leading to the highly porous hydroxide nanosheets. These reversible chemical processes bridge the gap between the
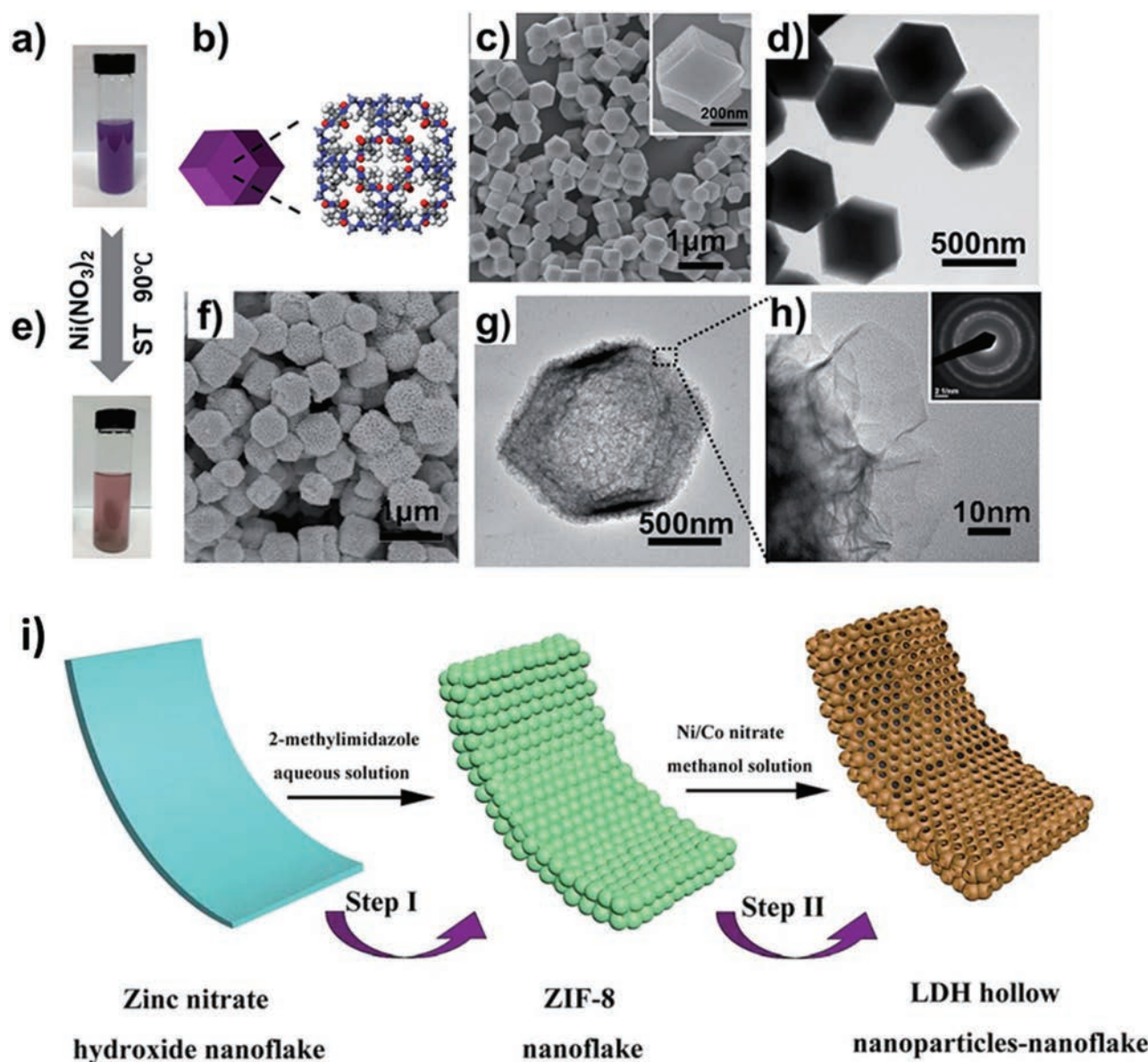

Figure 9. a–h) The synthesis of NiCo-LDH nanocages from ZIF-67. Reproduced with permission.[170] Copyright 2015, Royal Society of Chemistry. a) Digital photo of ZIF-67 solution. b) Geometrical and crystal structural models of ZIF-67. c) Low- and high-magnified (inset) SEM images. d) TEM image of ZIF-67. e) Digital photo of NiCo-LDH nanocages. f) SEM image of NiCo-LDH nanocages. g,h) TEM images of NiCo-LDH nanocages. The inset in figure (h) is the corresponding selective area electron diffraction (SAED) pattern. i) Schematic of the synthetic route from zinc nitrate hydroxide to Ni/Co-based hollow LDH arrays. Reproduced with permission.[172] Copyright 2016, Royal Society of Chemistry.
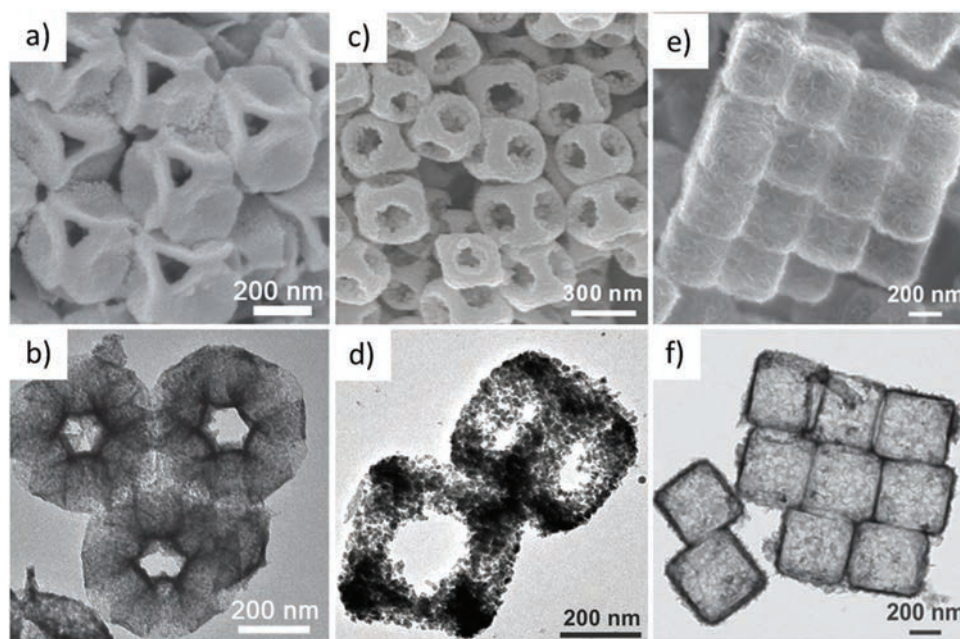
**ADVANCED
SCIENCE NEWS**

www.advancedsciencenews.com

**ADVANCED
ENERGY
MATERIALS**

www.advenergymat.de

Figure 10. a,b) SEM and TEM images of Ni–Co mixed oxide cages obtained by anisotropic ammonia etching Ni–Co PBA cubes and followed annealing of in air at 350 °C. Reproduced with permission.[174] Copyright 2016, John Wiley and Sons. c,d) SEM and TEM images of NiS nanoframes obtained by reacting Ni-Co PB analogue nanocubes with Na_2S at 100 °C for 6 h. Reproduced with permission.[175] Copyright 2015, John Wiley and Sons. e,f) SEM and TEM images of Ni–Co–MoS_2 nanoboxes produced from solvothermal reaction of ammonium tetrathiomolybdate on the surface of Ni–Co PBA nanocubes. Reproduced with permission.[176] Copyright 2016, John Wiley and Sons.

classic inorganic synthesis and the MOF-based nanofabrication, as we have illustrated in Figure 3a.[173] Prussian blue analog (PBA) nanocubes have also been used for fabricating porous inorganic nanomaterials. For example, by simply treating Ni–Co PBA nanocubes with ammonium at room temperature, the precursor cubes would undergo an unusual structural evolution and transform into a cage-like nanostructure, which can be further converted to Ni–Co mixed oxide cages by the calcination in air (**Figure 10**a,b).[174] The resulting Ni–Co mixed oxide cages exhibit the enhanced OER activity with a small overpotential of 0.38 V at a current density of 10 mA cm^{-2}, and the good durability in the alkaline medium. In another case, by dispersing Ni-Co PBA in a Na_2S solution, NiS nanoframes was obtained at an elevated temperature (Figure 10c,d).[175] From time-dependent morphology analysis, it is observed that the edges are first etched and a thin shell of NiS is formed locally at the position subjected to the ion exchange reaction with S^{2-}. No CoS is formed because the Co^{3+} cations are strongly complexed with CN^-. Well-defined Ni-Co-MoS_2 nanoboxes assembled by ultrathin nanosheets have also been obtained by reacting Ni-Co PBA with ammonium thiomolybdate (Figure 10e,f), which exhibits the enhanced electrochemical activity as an HER catalyst with an onset potential of 125 mV and a small Tafel slope of 51 mV dec^{-1}.[176]

All the above discussion indicates that MOF nanostructure can be directly converted into hierarchical oxide/hydroxide forms in well controlled style. Also, it is possible to further sculpture the morphology of MOFs during the material conversion process. It can be speculated that through these processes, a wide range of well-defined hierarchical hollow structures of transition metal compounds (such as sulfide, selenide, and

phosphide) can be synthesized from the basic oxide/hydroxide nanostructures.

4.4.3. Hierarchically Carbon-Supported Electrocatalysts from MOF

While calcination of MOFs under an inert or reductive atmosphere, the resulted products are quite different. The thermal condensation of the organic components would give the rise of carbon residuals. Ma et al.[177] have designed hybrid Co_3O_4-carbon porous nanowire arrays (denoted as Co_3O_4C-NAs) by the carbonization of $Co(C_{12}H_6O_4)\cdot(H_2O)_4$ MOFs under a N_2 atmosphere, as illustrated in **Figure 11**a. The Co_3O_4C-NAs are preserved with the wire-like morphology of the initial Co-based MOF and simultaneously numerous pores are produced within the nanowires. This novel oxygen evolution electrode can be operated in alkaline solutions, affording a low onset potential of 1.47 V vs RHE, a stable current density of 10.0 mA cm^{-2} at 1.52 V, and a small Tafel slop of 70 mV dec^{-1} in 0.1 M KOH solution (Figure 11b,c). The achieved ultrahigh OER activity and strong durability can then be ascribed to the unique nanowire array electrode configuration as well as the in situ carbon incorporation, which lead to the large active surface area, the enhanced capability for mass/charge transport and bubble release, and the excellent structural integrity. Chemical conversion of carbon-supported metal or metal oxide nanoparticles into phosphides provides a good strategy to obtain high-performance catalysts. Sun et al.[178] have developed porous Co-P/NCs nano-polyhedrons composed of CoP_x (a mixture of CoP and Co_2P) nanoparticles embedded in N-doped carbon from ZIF-67 by the carbonization and the subsequent phosphidation, as
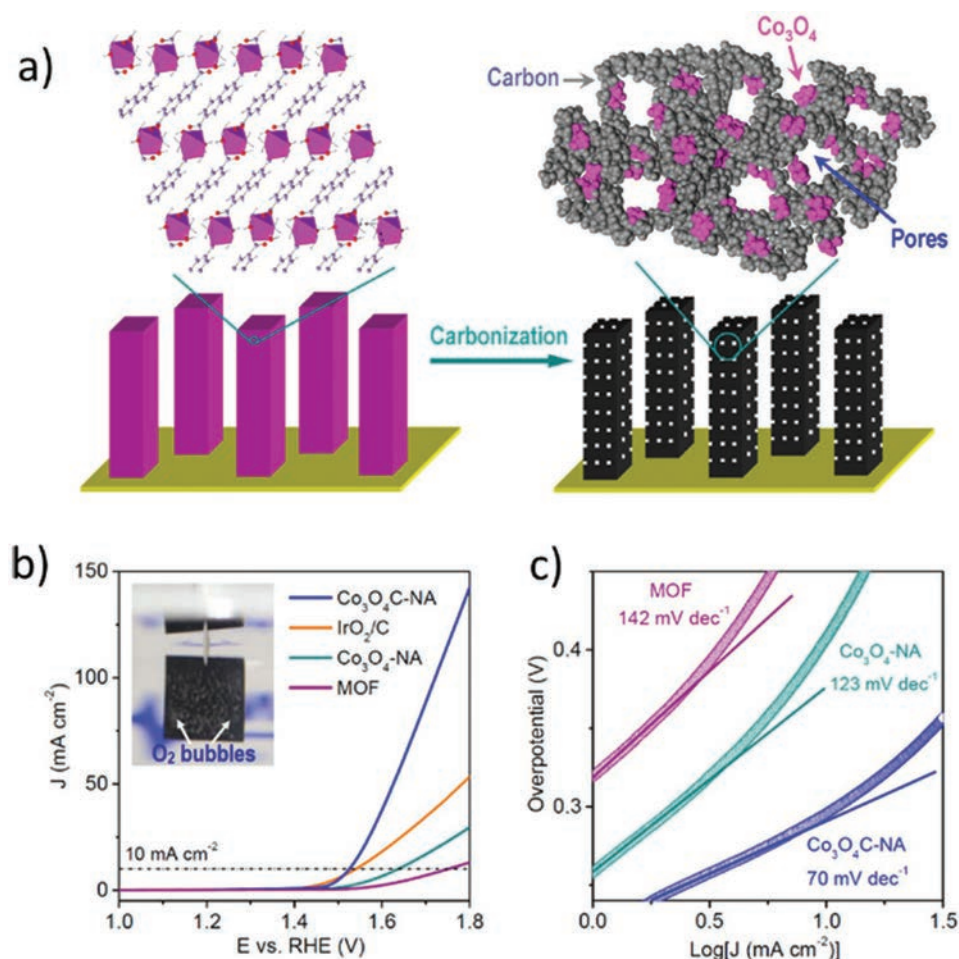
**ADVANCED
SCIENCE NEWS**
www.advancedsciencenews.com

**ADVANCED
ENERGY
MATERIALS**
www.advenergymat.de

Figure 11. a) Schematic illustration of fabrication of hybrid Co_3O_4-Carbon porous nanowire arrays (Co_3O_4C-NA). b) Polarization curves and c) Tafel plots of Co_3O_4C-NA, IrO_2/C, Co_3O_4-NA, and the MOF in an O_2-saturated 0.1 M KOH solution (scan rate 0.5 mV s^{-1}). Inset in (a): optical image of Co_3O_4C-NA used as the OER electrode operating at 1.70 V with generated bubbles on the surface. Reproduced with permission.[177] Copyright 2014, American Chemical Society.

illustrated in **Figure 12**a. The optimal Co-P/NCs show the high specific surface area of 183 m^2 g^{-1}, and exhibit the remarkable catalytic performance for both HER and OER in 1.0 M KOH, affording a current density of 10 mA cm^{-2} at low overpotentials of −154 mV for HER and 319 mV for OER, respectively (Figure 12b,c). However, this performance is not superior to that of the CoP hollow polyhedron catalyst derived by first oxidization and followed phosphidization from ZIF-67,[179] which can be owing to the presence of carbon overlayers on the CoP nanoparticles, hindering the contact of metallic active sites with the electrolyte. Nevertheless, this carbonization-phosphidation approach has also been adapted by other groups to develop electrocatalysts with the improved catalytic performance by modifying the MOF structures or precisely tuning/optimizing the reaction conditions.[156,180,181] In order to overcome the screening effect of the carbon coating layers, Zhou et al.[182] have developed a three-step carbonization–oxidation–selenylation procedure to attain highly porous electrocatalysts from ZIF-67 precursors (**Figure 13**a). Specifically, these electrocatalysts are mainly composed of $CoSe_2$ nanoparticles partially embedded in defective carbon nanotubes ($CoSe_2$@DC, Figure 13b,c). It

is found that the pre-oxidization strategy for both the diffusion process of Se atoms forming $CoSe_2$@DC and the introduction of defects into CNTs exposing their active sites is critical. Meanwhile, the porous carbon skeleton can also be maintained. Therefore, all these favorable characteristics would lead to the catalyst with the excellent HER activity, requiring small overpotentials of ≈40 mV to initiate the HER reaction and 132 mV to achieve a current density of 10 mA cm^{-2} in 0.5 M H_2SO_4, accordingly (Figure 13d).

4.4.4. Metal Carbide

Molybdenum carbide (Mo_2C) has been proven as a very active HER catalyst under both acidic and basic conditions.[44] Like many other catalysts, further improvement of the catalytic activity of Mo_2C can be achieved by designing well-defined nanostructures with the small crystalline size and high porosity. For instance, nanoporous β-Mo_2C nanowires have been prepared by the pyrolysis of MoO_x/amine hybrid nanowires, which yields the much lower onset overpotential and over 50 times
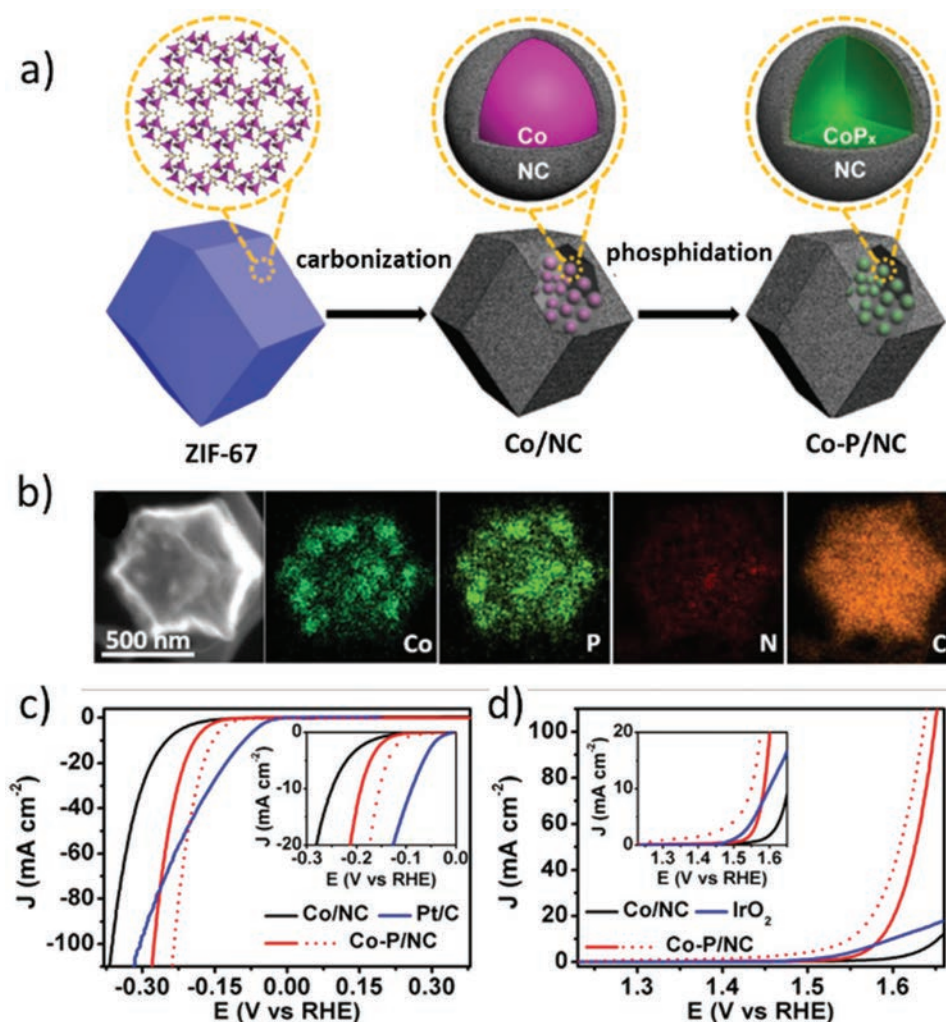
Figure 12. a) Schematic illustration of fabrication process of the CoP/NC nanohybrids. b) STEM and the elemental mapping images of Co-P/NC showing the element distributions. c) HER and d) OER polarization curves of Co/NC, Co-P/ NC, Pt/C, and IrO$_2$ in 1 M KOH. The solid and dotted red lines represent samples with loading amounts of 0.283 and 1.0 mg cm^{-2}, respectively. Reproduced with permission.[178] Copyright 2015, American Chemical Society.

larger current density at 200 mV than those of the commercial Mo$_2$C microparticles.[43] Lou et al. have further synthesized the well-designed porous MoC$_x$ nano-octahedrons[183] and the hierarchical β-Mo$_2$C nanotubes[184] by thermal conversion of molybdenum-based metal-organic frameworks (MOFs) and MoO$_3$-templated Mo-polydopamine nanorods, respectively, as shown in **Figure 14**a. The synthesis of MoC$_x$ nano-octahedrons relies on the confined and in situ carburization reaction occurring in a unique MOFs-based compound (NENU-5), consisting of a Cu-based MOFs (HKUST-1) host and Mo-based Keggin polyoxometalates (POMs) guest resided in pores, which enables the uniform formation of ultrafine MoC nanocrytallites embedded in an amorphous carbon matrix without any coalescence and excess growth (Figure 14b). Benefiting from the unique nanostructure, these porous MoC$_x$ nano-octahedrons reveal the remarkable electrocatalytic activity for HER in both acidic and basic solutions with the good stability. In contrast to use MOF as the precursor, the synthesis of hierarchical β-Mo$_2$C

nanotubes is first started with MoO$_3$ nanorods. Figure 14c,d give the synthetic route and TEM image of the hierarchical β-Mo$_2$C nanotubes, accordingly.[184] Mo-polydopamine hybrid nanotubes constructed by 2D ultrathin nanosheets are then synthesized by in situ polymerization of Mo-dopamine complex using MoO$_3$ nanorods as the self-degradable template and Mo source. The hierarchical β-Mo$_2$C nanotubes would be next obtained by directly carburizing the Mo-polydopamine nanotubes under an inert atmosphere. Due to the unique structural advantages, the as-prepared hierarchical β-Mo$_2$C nanotubes demonstrate the excellent electrocatalytic performance for hydrogen evolution in both acidic and alkaline conditions.

4.4.5. Summary on MOF-Directed Nanofabrication

The MOF-directed syntheses have been emerged as a unique class of nanofabrication approach which can be employed
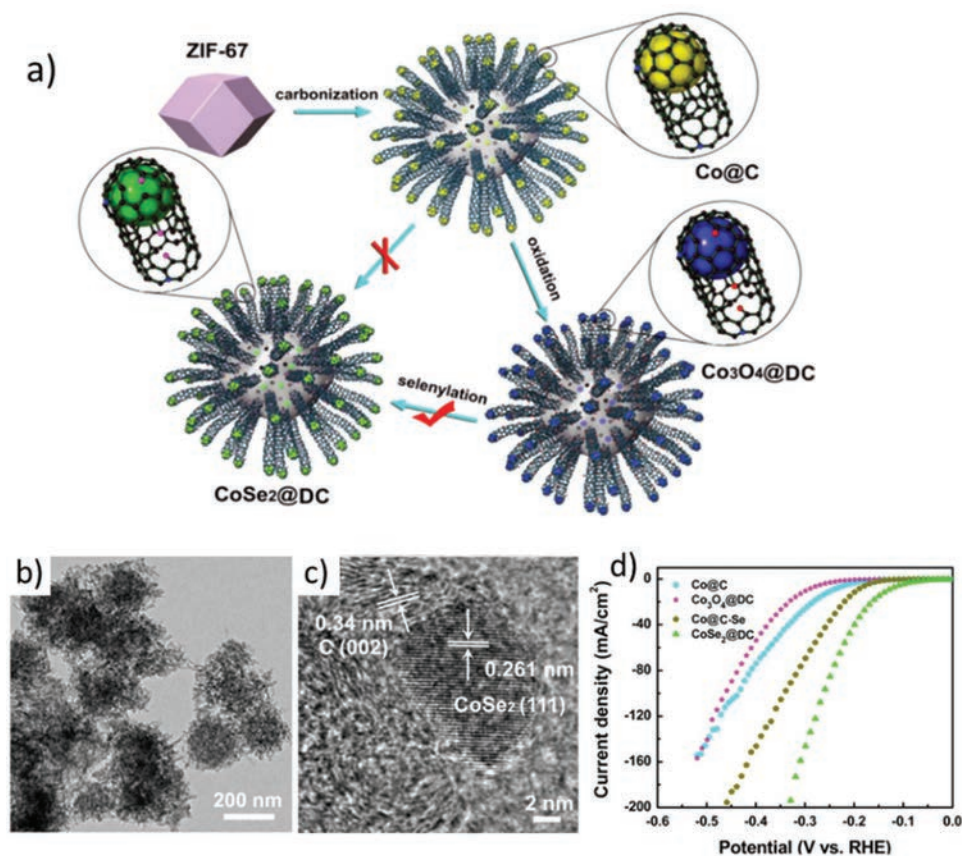
Figure 13. a) Schematic illustration of the synthetic procedure for $CoSe_2$@DC. b,c) TEM images of $CoSe_2$@DC. d) Polarization curves of the $CoSe_2$@DC catalyst and control samples. Reproduced with permission.[182] Copyright 2016, Elsevier Science Ltd.

complimentarily with other methods such as the hydrothermal synthesis and electrodepositions. The great tunability of the MOF synthesis and the subtle structure modulation under certain conditions would render this method great flexibility in the nanofabrication design.

5. Design of Hierarchical Nanostructures for PEC Water Splitting

5.1. General Considerations of Hierarchical Nanostructure for PEC Devices

In a PEC device, the major active material player is the semiconductor which is responsible for both light harvesting and charge separation. Oxide-based semiconductors, such as TiO_2, ZnO, $BiVO_4$, Fe_2O_3, and WO_3, are the most studied photoelectrode materials due to their suitable band edge positioning for using as a photoanode or a photocathode.[185] It is known that these materials either exhibit poor light absorption due to their large bandgap or have poor electro-hole separation capacity. As it has been discussed in Section 3.2, hierarchical nanostructures may offer many advantages as compared with their planar counterparts, in processes from light harvesting to charge separation. The enhancement effects of using hierarchical nanostructures have also been widely reported.[8,186–194] It is hard to choose a champion

device as different devices may have their own enhancement mechanisms. After introducing various synthesis techniques in the previous section, here we will focus more on the device structure and the performance-enhancement mechanisms.

5.2. Branched Nanostructures for PEC

Branched semiconductor nanostructures have been widely considered as ideal architectures for the applications in PEC water splitting because they can simultaneously offer the large contact area with electrolytes, the excellent light-harvesting capacity, and the highly conductive pathways for charge collection. Many synthetic methods can be employed for the synthesis of branched nanostructures, while the hydrothermal approach is the most frequently used scheme because of its low cost and high reproducibility for growth of well-defined nanostructures. Recently, Cho et al.[186] have designed a photoanode on FTO with hierarchically branched TiO_2 nanorod (B-NR) structures by utilizing a two-step hydrothermal growth approach. Each growth step is seeded with spin coated TiO_2 nanoparticles. **Figure 15**a,b display the SEM and TEM images of the branched nanostructures, respectively, revealing that the branches have cone-like shape and uniformly covering the surface of nanorods (NRs). It is observed that both NRs and B-NRs yield the higher light absorption than the NPs due to the antireflective effect,
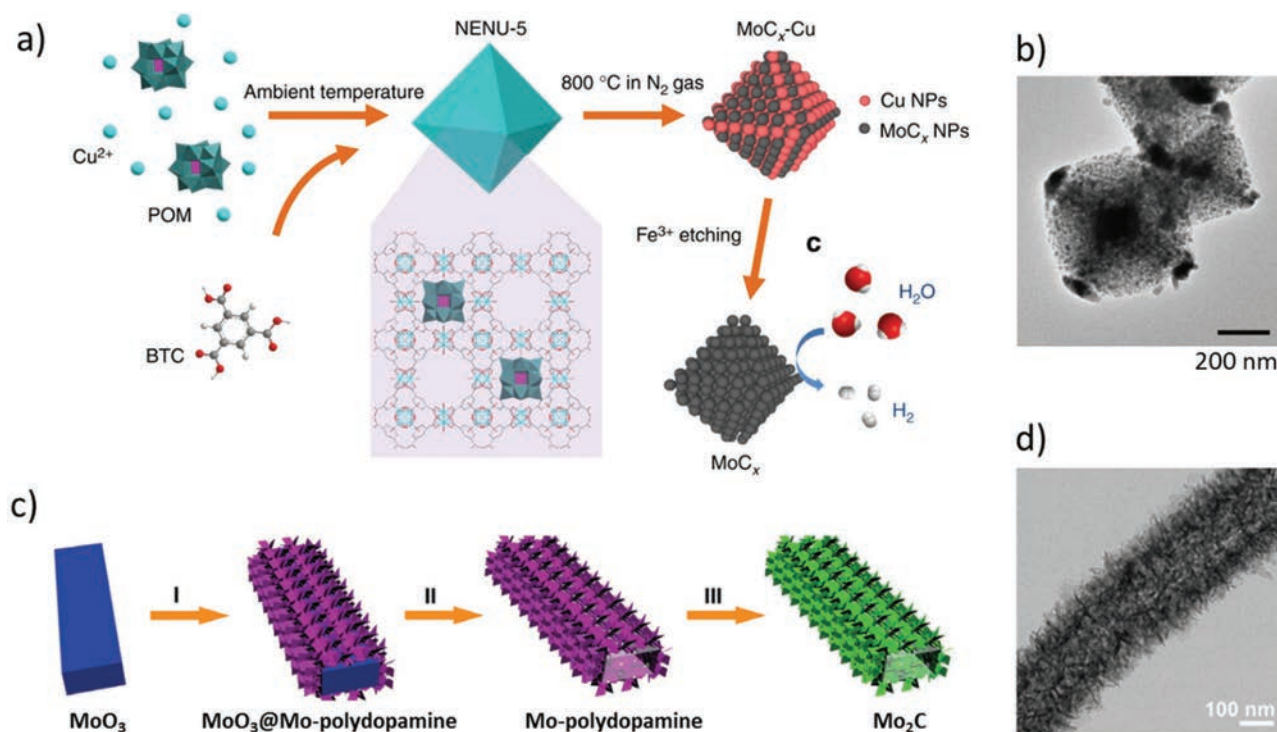
ADVANCED
SCIENCE NEWS
www.advancedsciencenews.com

ADVANCED
ENERGY
MATERIALS
www.advenergymat.de

Figure 14. a, b) Synthesis procedure and TEM image of porous MoC$_x$ nano-octahedrons. Reproduced with permission.[183] Copyright 2015, Nature Publishing Group. c,d) Synthesis procedure and TEM image of hierarchical β-Mo$_2$C nanotubes. Reproduced with permission.[184] Copyright 2015, John Wiley and Sons.
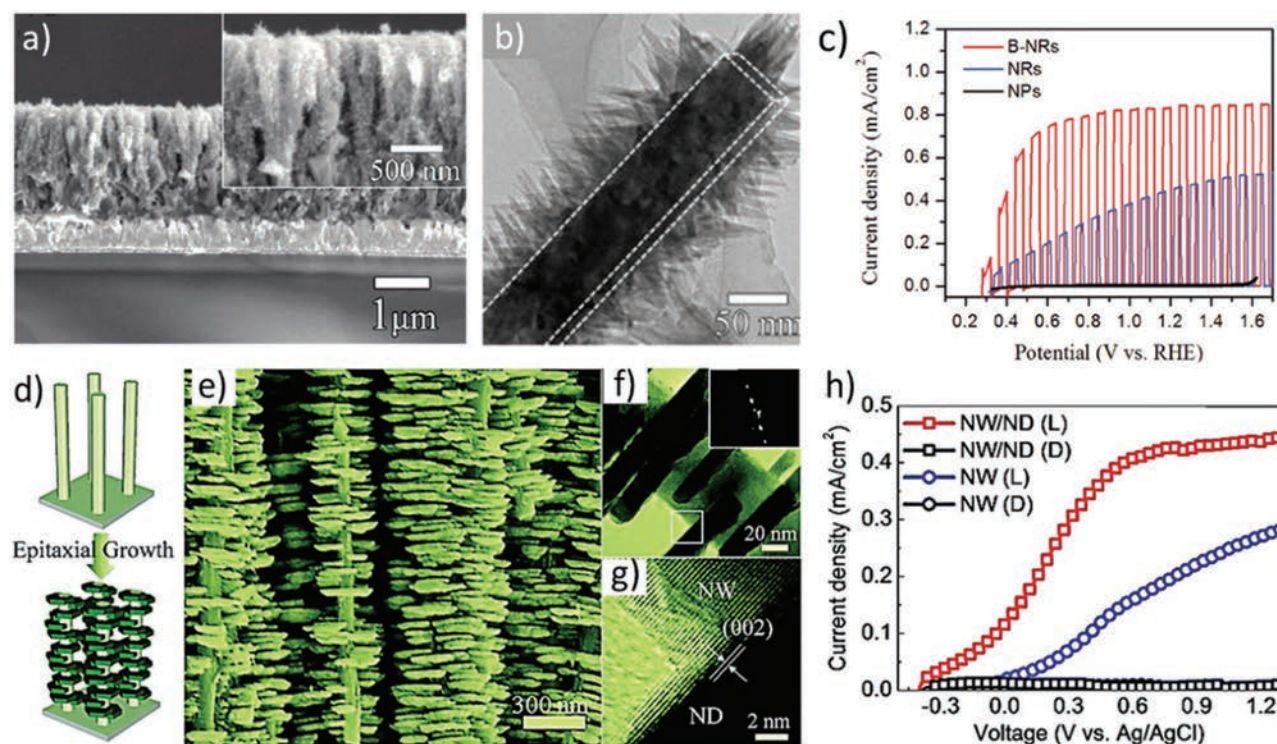

Figure 15. a) SEM and b) TEM images of branched TiO$_2$ nanorods (TiO$_2$ B-NRs). c) Chopped J–V curves of TiO$_2$ B-NRs, NRs, and NPs under Xenon lamp (UV portion of spectrum matched to AM 1.5G, 88 mW cm^{-2}) illumination. Reproduced with permission.[186] Copyright 2011, American Chemical Society. d) Schematic illustrating the epitaxial growth of ZnO ND on NW. e) SEM, f) TEM and g) HRTEM images of the single-crystalline ZnO NW/ND nanostructure. h) J–V curves of ZnO NW/ND and ZnO NW obtained in the dark (D) and under one-sun illumination (L). Reproduced with permission.[195]. Copyright 2014, John Wiley and Sons.

ADVANCED
SCIENCE NEWS

www.advancedsciencenews.com

**ADVANCED
ENERGY
MATERIALS**

www.advenergymat.de

which is the result of a graded refractive index and an increased light absorption path length. The PEC test also demonstrates that both NRs and B-NRs have the much better performance for solar assisted water oxidization, where the B-NRs photoanode exhibits the highest saturate current density, being almost double of the one of NRs photoanode (Figure 15c). Although the NPs have the largest TiO$_2$/electrolyte interfacial area, their light absorption and carrier transport are much less efficient, leading to a much lower incident photon-to-current conversion efficiencies (IPCE). The surface area of the B-NRs is about four times larger than that of the NRs, which can facilitate the whole transfer kinetics at the TiO$_2$/electrolyte interface for the water oxidization. In another report, Chen et al.[195] have demonstrated their construction of single-crystalline and branched nanowire arrays through a two-step hydrothermal growth of ZnO nanodisks (NDs) on ZnO nanowire (NWs) arrays. The NDs are grown perpendicular to the ZnO NWs through an epitaxial fashion, which not only increases the surface area and the light utilization, but also support the fast charge transport, leading to a four times higher power conversion efficiency than the one of primary NWs (Figure 15d–h).

5.3. Periodic/Patterned 3D Nanoarrays

Nanoarrays arranged in periodic micro-/nano-scale patterns represent an interesting class of hierarchically architectures that often exhibit the better performance than close packed nanowire arrays in PEC devices. For instance, pre-patterning a substrate enables radial alignment of the grown nanoarrays, which can improve the light harvesting capacity of the device

by providing multiple light scattering centers, and meanwhile increase the electrode surface area for contacting with the electrolyte. Wang et al.[190] have fabricated a photoelectrode consisting of the heterostructured TiO$_2$ nanorod@nanobowl (NR@NB) arrays with rutile TiO$_2$ nanorods grown on the inner surface of arrayed anatase TiO$_2$ nanobowls by a method combining interfacial nanosphere lithography and hydrothermal growth (**Figure 16**a,b). The TiO$_2$ NR@NB arrays are used as the photoanode with the significant improvement in the PEC performance for water splitting observed. The saturated photocurrent density of the NR@NB arrays can reach 1.24 mA cm^{-2} at 1.23 V versus RHE under AM 1.5G illumination, while the TiO$_2$ NR and nanobowl (NB) arrays only show 0.68 and 0.1 mA cm^{-2}, respectively, as shown in Figure 16c. This remarkable two-fold enhancement in PEC performance can be attributed to the improved light trapping and mass transport properties offered by the hierarchical NR@NB architectures, as well as the improved charge separation because of the anatase–rutile heterojunction. It is worthy to mention that such 3D periodic multiscale TiO$_2$ architectures can as well be constructed by patterning the seed layer using other cost-effective techniques, including nanoimprinting, interference lithography (IL), and soft-mask assisted photolithography, etc.[189,193,196,197]

5.4. Hierarchical Heterojunctions for PEC Water Splitting

Hierarchically structured heterojunctions can be viewed as an extended or complexed form of "core-shell" structures, which combines two different semiconductors by favorable band alignment that is able to improve the device light absorption,
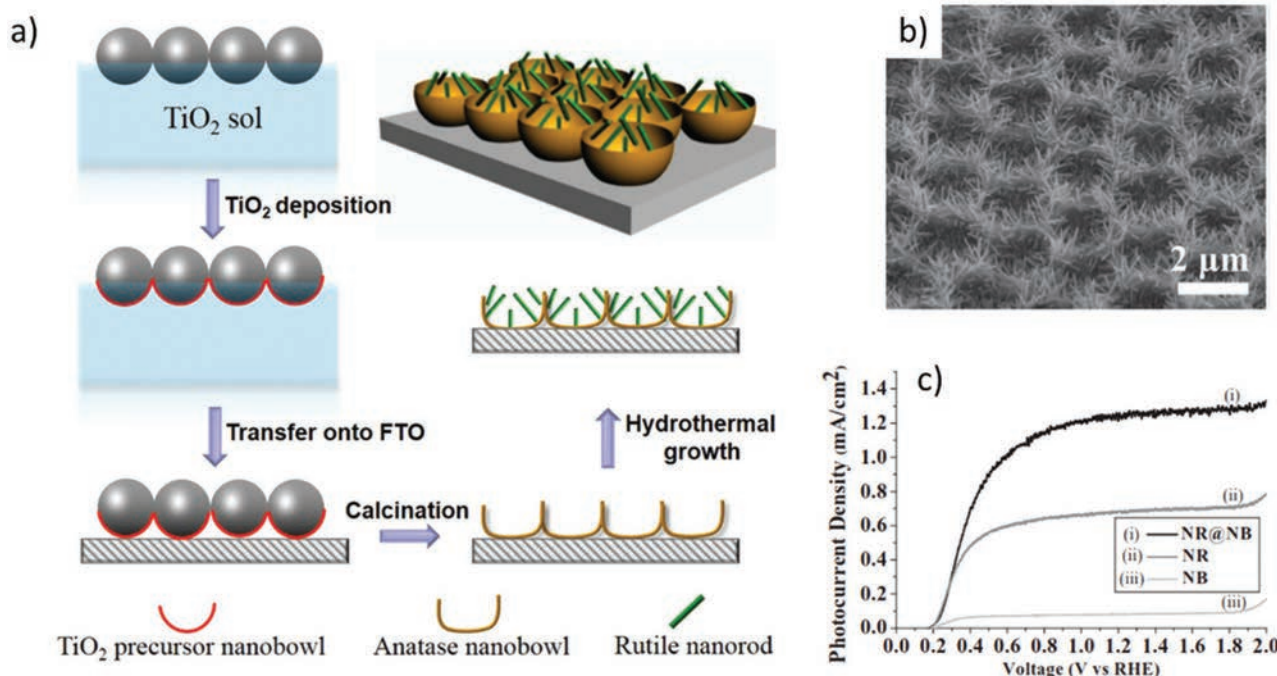

Figure 16. a) Schematic illustration of the preparation process of TiO$_2$ NR@NB arrays. b) SEM image of the TiO$_2$ NR@NB arrays. c) LSV curves of TiO$_2$ NB, NR, and NR@NB array electrodes recorded in a 1 M NaOH solution under simulated one sun illumination (AM 1.5G, 100 mW cm^{-2}). Reproduced with permission.[190] Copyright 2016, John Wiley and Sons.

**ADVANCED
SCIENCE NEWS**

www.advancedsciencenews.com
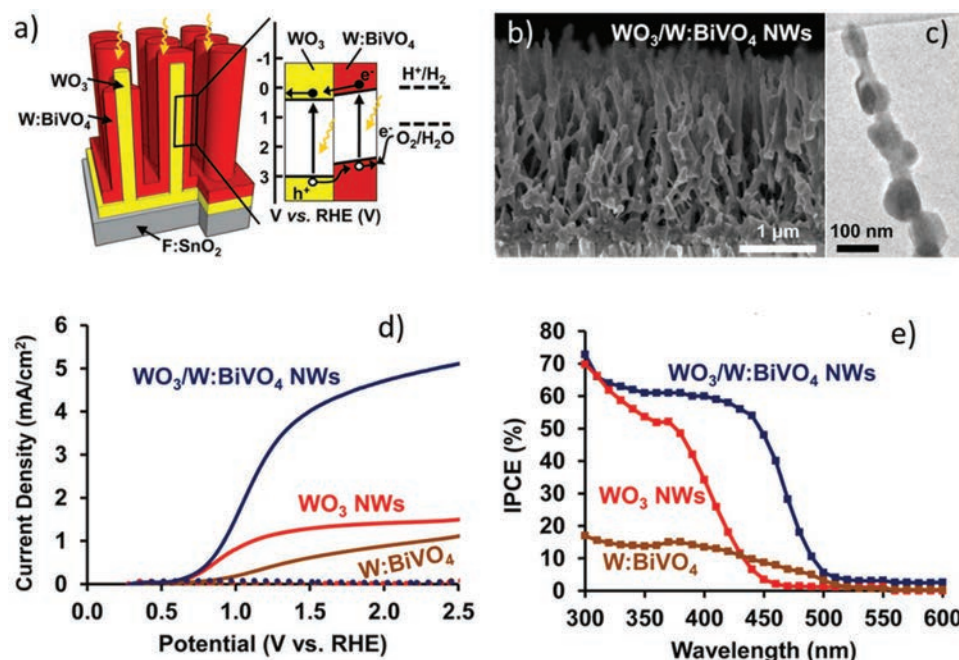
**ADVANCED
ENERGY
MATERIALS**

www.advenergymat.de

Figure 17. a) Structural schematic and energy band diagram of the core/shell NWs and type-II staggered heterojunction, in which charges generated in both the W:BiVO4 shells and WO3 NW cores can contribute to the water oxidation photocurrent. b,c) SEM and TEM images of WO_3/W:BiVO$_4$ hybrid nanowires. d) J–V curves of the WO_3/W:BiVO$_4$ NW photoanode and control samples measure under AM 1.5 G illumination in 0.5 M potassium phosphate electrolyte buffered to pH of 8. e) IPCE curves measured at 1.23 vs RHE. Reproduced with permission.[198] Copyright 2014, American Chemical Society.

charge separation and surface charge transfer properties. As compared to the ideal "core-shell" heterojunctions, the hierarchically structured heterojunctions can be obtained much easier as the lattice mismatch problems are eliminated. The type-II band alignment that has the staggered gap is a very useful configuration for the efficient charge separation. Rao et al.[198] have demonstrated a type-II WO_3/BiVO$_4$ core/shell nanowires based photoanode by coating a thin layer of BiVO$_4$ onto a vertical array of electrically conductive WO_3 nanowires (NWs, **Figure 17**a–c), in which the BiVO$_4$ is the primary light absorber and WO_3 acts as an electron conductor. In details, the WO_3 NWs are synthesized on FTO by flame vapor deposition and the BiVO$_4$ nanoparticles are decorated on the WO_3 NWs by drop casting. After annealing, W can diffuse into BiVO$_4$ to form a gradient W-doped layer (denoted as W:BiVO$_4$). Impressively, the photocurrent of the WO_3/W:BiVO$_4$ hybrid NWs as illustrated in the J–V curve (Figure 17d) can reach 3.1 mA cm^{-2} at 1.23 V versus RHE under AM 1.5G illumination, which is more than twice the sum of the separate photocurrents of the bare WO_3 NW array and a "same-mass W:BiVO$_4$ film", indicating a powerful synergistic effect between the WO_3 core and the W:BiVO$_4$ shell. This synergy is also evident in the corresponding performance enhancement in the IPCE results (Figure 17e).

5.5. Plasmonic Effect for Performance Enhancement in PEC Water Splitting

The surface plasmon resonance (SPR) effect, which is the coherent collective oscillation of conduction electrons

surrounding the metallic surfaces, has attracted much attention as a route to improve the solar energy conversion efficiency of photovoltaic devices due to its advantageous optical properties.[199–210] Plasmonic enhancement is achieved mainly through three mechanisms, including far-field scattering, near-field enhancement, and charge carrier or resonant energy transfer.[206] Subwavelength-sized nanoparticles of noble metals such as Au and Ag can exhibit strong localized surface plasmon resonances (LSPRs) at the wavelengths range from UV, visible to near infrared (NIR), depending on the kind of material, their size, particle aspect ratio, and the environment.[211,212] Although significant progress has been made in utilization of plasmonic nanostructures can be optimized to increase the light absorption, it is still very challenging to effectively collect the energy harvested due to the weak coupling between the plasmonic nanostructure and the semiconductor. Recently, Li et al.[213] have made a ground-breaking study on the utilization of plasmonic effect to concentrate the incident light into hematite nanorods, which significantly improves the PEC performance for water splitting. **Figure 18**a,b illustrate the typical design of such heterostructure, which is consisted of a hematite nanorod arrays grown on a plasmonic gold nanohole arrayed pattern. The hole width, pitch and the Au film thickness are chosen to enable the excitation of both the surface plasmon polaritons (SPP) and LSPR modes at the wavelengths below and above the band gap of hematite, respectively. When the hematite nanorods are grown on the Au nanohole arrays, an increase in absorption across the entire spectral range is clearly observed as compared with the hematite on bare FTO (Figure 18c), and meanwhile, an approximately ten-fold increase is in the photocurrent at a
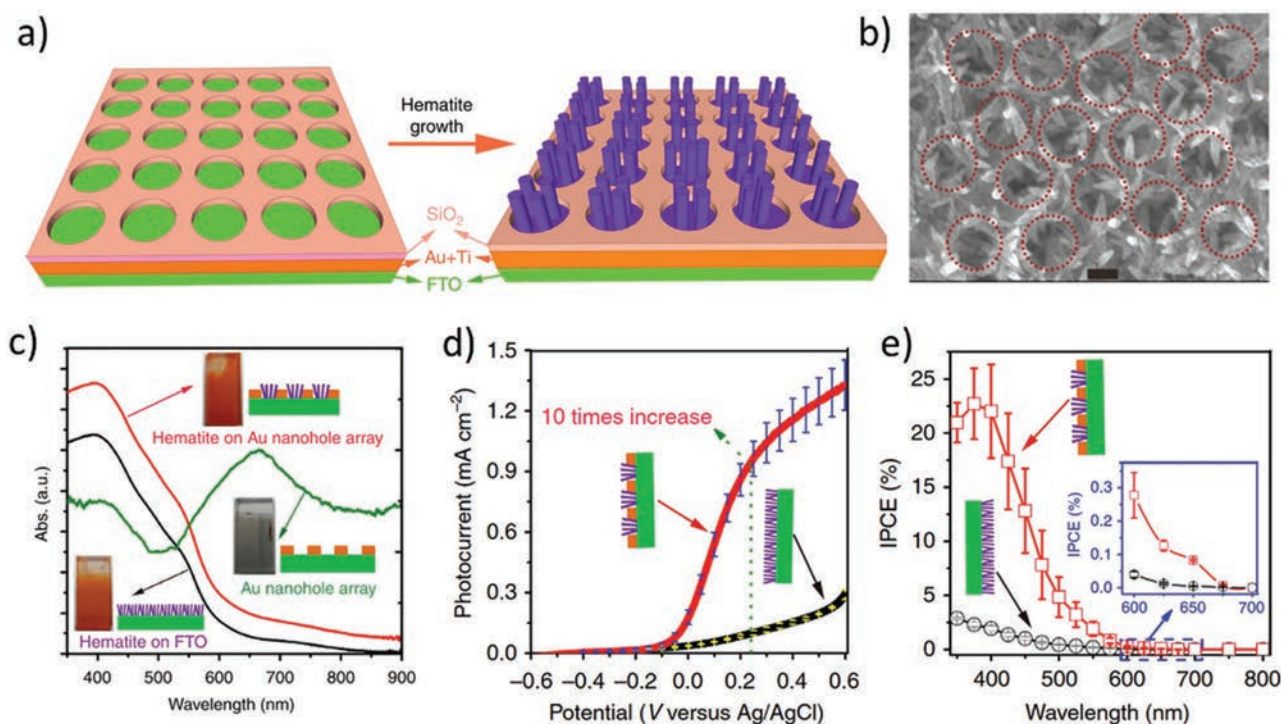
Figure 18. a) Scheme for the growth of the hematite nanorod array on the Au nanohole array. b) Scanning electron microscopic images of Au nanohole array with hematite nanorods (scale bars: 1 µm). c) Ultraviolet–visible absorption spectra for 150-nm long hematite nanorods on the bare FTO and on the Au nanohole array pattern, respectively. d) J–V curves under 1 sun illumination. e) IPCE spectra; the insert is the IPCE in 600–700 nm range. Reproduced with permission.[213] Copyright 2013, Nature Publishing Group.

bias of 0.23 V versus Ag/AgCl under simulated solar radiation in 1 M KOH (Figure 18d). Substantial enhancement of IPCE in the wavelength ranging from 325 to 700 nm has been witnessed with two distinct enhancement peaks of at 425 and 650 nm, respectively (Figure 18e). These positions correlate well with the enhanced transmission and absorption of the Au nanohole arrays, which corresponds to the SPP and LSPR mode as confirmed by finite difference time domain (FDTD) simulations. While the SPP-induced resonant energy transfer is responsible for the enhancement at the energies below the band edge of the hematite, the SPP mode would lead to the extraordinary optical transmission through the nanohole array and then launch a guided wave mode inside the nanorods, further enhancing the light absorption.

5.6. Catalysts Integration

The PEC water splitting process is typically referred to the integration of solar energy conversion and water electrolysis (or the half HER and/or OER reaction) in a single photoelectrode. An efficient PEC system should have all the steps, including the light harvesting, the electron-hole pair generation, the charge separation and transport, and the surface water oxidation/reduction reaction proceeded efficiently. Thus, integration of catalysts onto the photoelectrode would be very beneficial for the performance improvement. Generally, the catalyst should be as thin as possible in order to reduce the parasitic light absorption losses caused by the catalyst, and at the same time,

the catalyst should have the maximized surface area to expose more catalytic sites. A wide range of thin film deposition techniques can be chosen for this purpose, including dry methods of sputtering, thermal/electron-beam evaporation, atomic layer deposition (ALD) and chemical vapor deposition; and the wet methods of spin coating, self-assembly, hydrothermal, and electrodeposition. Ning et al.[214] have presented an interesting work on the catalyst integration that is capable to simultaneously enhance the charge separation and the water oxidation efficiency of photoanodes by introducing reduced graphite oxide (rGO) and NiFe-layered double hydroxide (LDH) on TiO_2 nanorod arrays (NAs). In specific, well-aligned NA photoanode is first fabricated by the spin-coating of graphene nanosheets onto the surface of TiO_2 NAs, followed by the subsequent electrodeposition of NiFe-layered double hydroxide (LDH) nanoplatelets (**Figure 19**a,b). The resulting ternary TiO2/rGO/NiFe-LDH NA electrode yields a negatively shifted onset potential at −0.3 V in relative to the TiO_2/rGO NAs under a 150 W Xe lamp illumination at a power density of 100 mW cm^{-2}, and for a fair and consistent comparison, the photocurrent density of 1.74 mA cm^{-2} at 0.6 V, represents the highest value already among all four possible types of heterogeneously integrated photoanodes here, namely the TiO$_2$/rGO/NiFe-LDH, TiO$_2$/rGO, TiO$_2$/NiFe-LDH, and pristine TiO$_2$ NAs (Figure 19c). Based on the XPS analysis and DFT simulations, it is revealed that the rGO with a high work function can enable fast electron transportations by accepting photo-generated electrons from TiO$_2$, while the NiFe-LDH can then act as the co-catalyst, accelerating the surface water oxidation reaction (Figure 19d). As
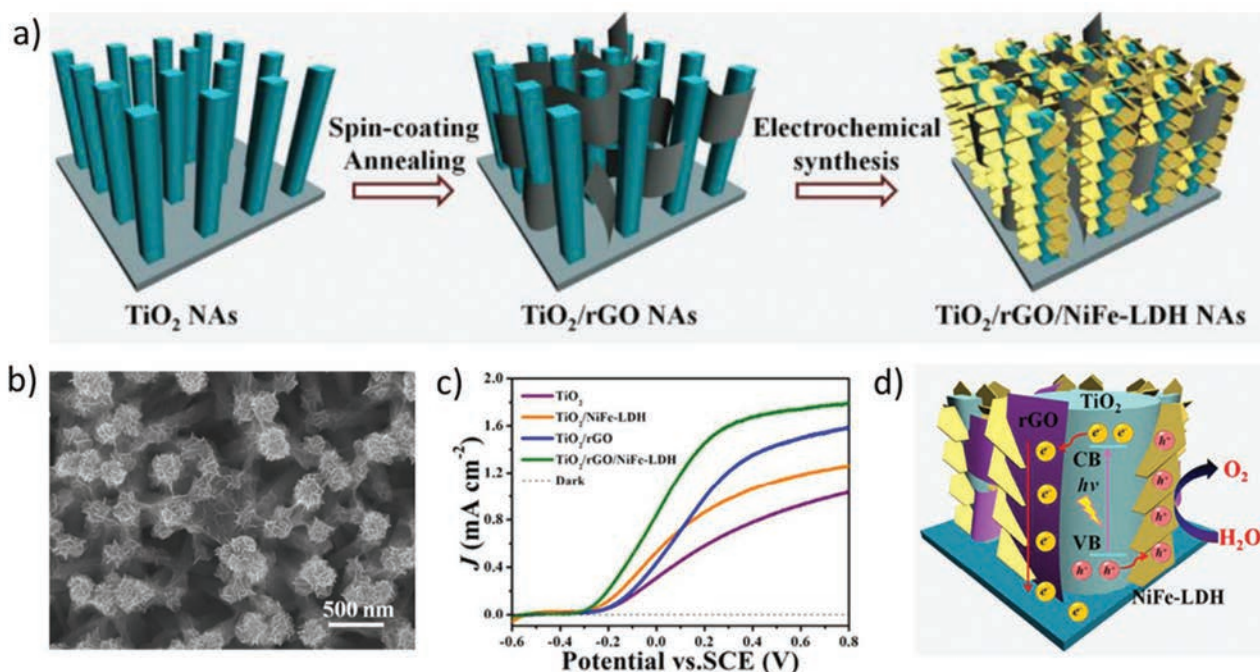
ADVANCED
SCIENCE NEWS
www.advancedsciencenews.com

ADVANCED
ENERGY
MATERIALS
www.advenergymat.de

Figure 19. a) Schematic illustration for the fabrication of TiO_2/rGO/NiFe-LDH core-shell NAs. b) SEM image of TiO_2/rGO/NiFe-LDH core-shell NAs. c) LSV curves measured under a 150 W Xe lamp illumination with a power density of 100 mW cm^{-2} on the photoanode in 0.5 M Na_2SO_4 aqueous solution. d) Schematic illustration for the PEC water oxidation process in the TiO_2/rGO/NiFe-LDH core-shell NAs photoanode. Reproduced with permission.[214] Copyright 2016, Royal Society of Chemistry.

a result, a synergistic effect can be effectively achieved by the integration of rGO and NiFe-LDH with TiO_2.

6. Conclusion and Perspective

Sustainable water splitting provides a promising way to resolve the problems related to continuous and enhanced consumption of fossil fuels. Realization of this sustainability, however, would rely on the successful development of low-cost and high-performance electrode materials. In addition to exploring materials that have high intrinsic activities, reconstruction of the materials in different arrangements also provides numerous possibilities for the performance enhancement. In this review, we have summarized the fabrication and the utilization of hierarchical nanostructures in electrochemical and photoelectrochemical water splitting devices. We have surveyed on the recent literature in broad topics related to hierarchical nanomaterials, in wish to extract the general strategies that would be used in the material design for electrocatalysts and PEC devices. We take the examples based on their structural novelty and methodological reliability in fabrications. Specifically, we have emphasized on three classes of powerful synthetic techniques, including hydrothermal reaction, electrodeposition, and MOF-templated synthesis, because these techniques can be simply employed to finish most of the synthesis tasks associated with the electrocatalytic and PEC applications. For instance, the hydrothermal method can be utilized to synthesize almost all the transition metal-based hierarchical nanomaterials via the autogenous self-organization or using a proper template. For that, we have demonstrated the design of self-organization flower-like architectures and various substrate (e.g., CNT, graphene, carbon fiber paper, and nickel foam)-supported hierarchical structures. The electrodeposition method has also been introduced for their versatility in producing dendrite-like nanostructures at mild processing conditions. We have as well highlighted the fabrication of various porous or hollow architectures by using well-defined MOF nanostructures as the self-sourced templates. To further facilitate the selection on the specific method for material syntheses, we compiled a table (Table S1, Supporting Information) that compares these synthetic methods based on the applicable materials, resulting morphologies, material performances and the methodological advantages. Undoubtedly, combining these methods with other chemical processes, such as selective etching, chemical bath deposition, and chemical vapor deposition (CVD) would allow more diversified material fabrications.

After establishing a knowledge framework about how to synthesize hierarchical nanostructures, in the next part related to PEC, we shift the emphasis onto the design of photoelectrodes and the beneficial effects of hierarchical structures in performance improvement. Obviously, the hydrothermal method shows unique advantages in morphology manipulations. In particular, it is possible to grow high-quality nanocrystals at specific position by pre-seeding, which extends the capacity in nanostructure fabrication. In fact, almost all oxide-based semiconductor nanostructures can be synthesized by the hydrothermal method, so that we can utilize it to obtain various hierarchical architectures by multi-step growth or area-selective pre-seeding. Electrodeposition is not

as versatile as the hydrothermal method in fabricating semiconductor nanostructures, but it is useful for catalyst loading and surface modification. We have demonstrated a few types of hierarchical structures that can be adopted in PEC devices, including branched, periodic/patterned, heterojunctional, plasmonic enhanced and catalyst-integrated nanoarrays. Through these examples we have illustrated that the hierarchical structure could improve the performance of photoelectrodes through the following mechanisms: 1) increasing the harvesting of photons with energy smaller than the bandgap through antireflective effect due to the graded effective reflective index; 2) increasing the broadband light absorption by incorporating a second semiconductor material or plasmonic nanostructures; 3) improving the charge separation by providing the integrated conduction path and the large surface area; and 4) accelerating HER or OER reaction by loading highly active catalysts onto the photoelectrode surfaces. Hierarchical nanostructures are also well suited to monolithic tandem PEC devices for achieving full water splitting, although the design of such devices still requires substantial efforts from material selection to device fabrication in order to ensure that the band structures of semiconductors involved are properly positioned and the currents produced by the different parts are well matched.

While highlighting the fabrication methods, we have paid less attention to the stabilities of the materials. Nevertheless, the stability of a material is always sensitive to the environment to which it is exposed and is more related to the intrinsic property of the material. It should be noted that, although hierarchical nanostructures offer many advantages in both electrocatalyst and PEC reactions, they also have some drawbacks. For example, when these structures are used in PEC devices, the high surface area would also induce the increased surface recombination (e.g., electron-hole pair recombination), leading to the reduction of photocurrent and fill factor of devices. In this case, the optimal surface passivation scheme is critical, and thin film deposition technologies, such as CVD, atomic layer deposition (ALD) and self-assembled monolayers could be adopted for the passivation purpose. Another important yet often ignored issue in PEC application is the pursuit of optimal morphology while underrating the crystal qualities during material synthesis. Sometimes, the conditions for fabricating the secondary structure would cause degradation to the primary structure. For example, the growth of nanostructure on silicon via hydrothermal means would often lead to surface oxidization or corrosion of its surface, producing an insulating 'dead layer' at the interface. In other cases, the component in the second layer may have the adverse doping effect to the primary structure, resulting in reduced device performance. Therefore, carefully choosing the materials system and the engineering process is crucial to the effective utilization of hierarchical nanostructures.

Supporting Information

Supporting Information is available from the Wiley Online Library or from the authors.

Conflict of Interest

The authors declare no conflict of interest.

[1] N. S. Lewis, D. G. Nocera, *Proc. Natl. Acad. Sci. U. S. A.* **2006**, *103*, 15729.

[2] M. G. Walter, E. L. Warren, J. R. McKone, S. W. Boettcher, Q. Mi, E. A. Santori, N. S. Lewis, *Chem. Rev.* **2010**, *110*, 6446.

[3] H. A. Gasteiger, S. S. Kocha, B. Sompalli, F. T. Wagner, *Appl. Catal. B Environ.* **2005**, *56*, 9.

[4] H. A. Gasteiger, N. M. Markovi , *Science* **2009**, *324*, 48.

[5] F. E. Osterloh, *Chem. Soc. Rev.* **2013**, *42*, 2294.

[6] C. C. L. McCrory, S. Jung, J. C. Peters, T. F. Jaramillo, *J. Am. Chem. Soc.* **2013**, *135*, 16977.

[7] C. C. L. McCrory, S. Jung, I. M. Ferrer, S. M. Chatman, J. C. Peters, T. F. Jaramillo, *J. Am. Chem. Soc.* **2015**, *137*, 4347.

[8] H. Chen, S. Yang, W. Chen, Y. Qiu, S. Yang, M. A. Butler, D. S. Ginley, R. Memming, A. J. Bard, P. V. Kamat, M. Gratzel, *Nanoscale Horiz.* **2016**, *1*, 96.

[9] H. M. Chen, C. K. Chen, R.-S. Liu, L. Zhang, J. Zhang, D. P. Wilkinson, *Chem. Soc. Rev.* **2012**, *41*, 5654.

[10] D. Lee, C. L. Grigoropoulos, in *Hierarchical Nanostructures for Energy Devices*, **2015**, pp. 175–200.

[11] B. You, N. Jiang, M. Sheng, M. W. Bhushan, Y. Sun, *ACS Catal.* **2016**, *6*, 714.

[12] C. G. Morales-Guio, L. Stern, X. Hu, *Chem. Soc. Rev.* **2014**, *43*, 6555.

[13] Z. W. Seh, J. Kibsgaard, C. F. Dickens, I. Chorkendorff, J. K. Nørskov, T. F. Jaramillo, *Science* **2017**, *355*, eaad4998.

[14] C. González-Buch, I. Herraiz-Cardona, E. M. Ortega, J. García-Antón, V. Pérez-Herranz, *Chem. Eng. Trans.* **2013**, *32*, 865.

[15] M. M. Jaksic, *Int. J. Hydrogen Energy* **2001**, *26*, 559.

[16] R. Solmaz, G. Karda , *Int. J. Hydrogen Energy* **2011**, *36*, 12079.

[17] M. Wang, Z. Wang, X. Yu, Z. Guo, *Int. J. Hydrogen Energy* **2015**, *40*, 2173.

[18] M. Fang, W. Gao, G. Dong, Z. Xia, S. Yip, Y. Qin, Y. Qu, J. C. Ho, *Nano Energy* **2016**, *27*, 247.

[19] S. Anantharaj, S. R. Ede, K. Sakthikumar, K. Karthick, S. Mishra, S. Kundu, *ACS Catal.* **2016**, *6*, 8069.

[20] G. Li, D. Zhang, Q. Qiao, Y. Yu, D. Peterson, A. Zafar, R. Kumar, S. Curtarolo, F. Hunte, S. Shannon, Y. Zhu, W. Yang, L. Cao, *J. Am. Chem. Soc.* **2016**, *138*, 16632.

[21] R. Ye, P. del Angel-Vicente, Y. Liu, M. J. Arellano-Jimenez, Z. Peng, T. Wang, Y. Li, B. I. Yakobson, S.-H. Wei, M. J. Yacaman, J. M. Tour, *Adv. Mater.* **2016**, *28*, 1427.

[22] A. B. Laursen, T. Pedersen, P. Malacrida, B. Seger, O. Hansen, P. C. K. Vesborg, I. Chorkendorff, *Phys. Chem. Chem. Phys.* **2013**, *15*, 20000.

[23] H. Vrubel, D. Merki, X. Hu, *Energy Environ. Sci.* **2012**, *5*, 6136.

[24] H. Wang, Z. Lu, S. Xu, D. Kong, J. J. Cha, G. Zheng, P.-C. Hsu, K. Yan, D. Bradshaw, F. B. Prinz, Y. Cui, *Proc. Natl. Acad. Sci. U. S. A.* **2013**, *110*, 19701.

[25] X. Zhang, F. Meng, S. Mao, Q. Ding, M. J. Shearer, M. S. Faber, J. Chen, R. J. Hamers, S. Jin, *Energy Environ. Sci.* **2015**, *8*, 862.

[26] M.-R. Gao, J.-X. Liang, Y.-R. Zheng, Y.-F. Xu, J. Jiang, Q. Gao, J. Li, S.-H. Yu, *Nat. Commun.* **2015**, *6*, 5982.

[27] Y. Sun, C. Liu, D. C. Grauer, J. Yano, J. R. Long, P. Yang, C. J. Chang, *J. Am. Chem. Soc.* **2013**, *135*, 17699.

[28] P. D. Tran, S. Y. Chiam, P. P. Boix, Y. Ren, S. S. Pramana, J. Fize, V. Artero, J. Barber, *Energy Environ. Sci.* **2013**, *6*, 2452.

[29] D. Kong, H. Wang, Z. Lu, Y. Cui, *J. Am. Chem. Soc.* **2014**, *136*, 4897.

[30] K. Wang, D. Xi, C. Zhou, Z. Shi, H. Xia, G. Liu, G. Qiao, *J. Mater. Chem. A* **2015**, *3*, 9415.

[31] Q. Dong, Q. Wang, Z. Dai, H. Qiu, X. Dong, *ACS Appl. Mater. Interfaces* **2016**, *8*, 26902.

[32] R. Zhang, X. Wang, S. Yu, T. Wen, X. Zhu, F. Yang, X. Sun, X. Wang, W. Hu, *Adv. Mater.* **2016**, *29*, 1605502.

[33] M. S. Faber, M. a Lukowski, Q. Ding, N. S. Kaiser, S. Jin, *J. Phys. Chem. C* **2014**, *118*, 21347.

[34] Z. Xing, Q. Liu, A. M. Asiri, X. Sun, *Adv. Mater.* **2014**, *26*, 5702.

[35] J. Tian, Q. Liu, A. M. Asiri, X. Sun, *J. Am. Chem. Soc.* **2014**, *136*, 7587.

[36] J. Kibsgaard, C. Tsai, K. Chan, J. D. Benck, J. K. Nørskov, F. Abild-Pedersen, T. F. Jaramillo, *Energy Environ. Sci.* **2015**, *8*, 3022.

[37] G. Zhang, G. Wang, Y. Liu, H. Liu, J. Qu, J. Li, *J. Am. Chem. Soc.* **2016**, *138*, 14686.

[38] X. Wang, Y. V. Kolen'ko, X.-Q. Bao, K. Kovnir, L. Liu, *Angew. Chem. Int. Ed.* **2015**, *54*, 8188.

[39] J. Tian, Q. Liu, A. M. Asiri, X. Sun, *J. Am. Chem. Soc.* **2014**, *136*, 7587.

[40] L. Liao, S. Wang, J. Xiao, X. Bian, Y. Zhang, M. D. Scanlon, X. Hu, Y. Tang, B. Liu, H. H. Girault, *Energy Environ. Sci.* **2014**, *7*, 387.

[41] J.-S. Li, Y. Wang, C.-H. Liu, S.-L. Li, Y.-G. Wang, L.-Z. Dong, Z.-H. Dai, Y.-F. Li, Y.-Q. Lan, *Nat. Commun.* **2016**, *7*, 11204.

[42] M. C. Weidman, D. V. Esposito, Y. C. Hsu, J. G. Chen, *J. Power Sources* **2012**, *202*, 11.

[43] L. Liao, S. Wang, J. Xiao, X. Bian, Y. Zhang, M. D. Scanlon, X. Hu, Y. Tang, B. Liu, H. H. Girault, *Energy Environ. Sci.* **2014**, *7*, 387.

[44] H. Vrubel, X. Hu, *Angew. Chem. Int. Ed.* **2012**, *51*, 12703.

[45] K. Xu, P. Chen, X. Li, Y. Tong, H. Ding, X. Wu, W. Chu, Z. Peng, C. Wu, Y. Xie, *J. Am. Chem. Soc.* **2015**, *137*, 4119.

[46] S. Wang, H. Ge, S. Sun, J. Zhang, F. Liu, X. Wen, X. Yu, L. Wang, Y. Zhang, H. Xu, J. C. Neuefeind, Z. Qin, C. Chen, C. Jin, Y. Li, D. He, Y. Zhao, *J. Am. Chem. Soc.* **2015**, *137*, 4815.

[47] W.-F. Chen, K. Sasaki, C. Ma, A. I. Frenkel, N. Marinkovic, J. T. Muckerman, Y. Zhu, R. R. Adzic, *Angew. Chem.* **2012**, *124*, 6235.

[48] C. Tang, L. Gan, R. Zhang, W. Lu, X. Jiang, A. M. Asiri, X. Sun, J. Wang, L. Chen, *Nano Lett.* **2016**, *16*, 6617.

[49] N.-T. Suen, S.-F. Hung, Q. Quan, N. Zhang, Y.-J. Xu, H. M. Chen, *Chem. Soc. Rev.* **2017**, *46*, 337.

[50] I. C. Man, H.-Y. Su, F. Calle-Vallejo, H. A. Hansen, J. I. Martínez, N. G. Inoglu, J. Kitchin, T. F. Jaramillo, J. K. Nørskov, J. Rossmeisl, *ChemCatChem* **2011**, *3*, 1159.

[51] C. C. L. McCrory, S. Jung, J. C. Peters, T. F. Jaramillo, *J. Am. Chem. Soc.* **2013**, *135*, 16977.

[52] M. Bajdich, M. García-Mota, A. Vojvodic, J. K. Nørskov, A. T. Bell, *J. Am. Chem. Soc.* **2013**, *135*, 13521.

[53] B. M. Hunter, J. D. Blakemore, M. Deimund, H. B. Gray, J. R. Winkler, A. M. Müller, *J. Am. Chem. Soc.* **2014**, *136*, 13118.

[54] J. Landon, E. Demeter, N. İnoğlu, C. Keturakis, I. E. Wachs, R. Vasić, A. I. Frenkel, J. R. Kitchin, *ACS Catal.* **2012**, *2*, 1793.

[55] J. W. D. Ng, M. García-Melchor, M. Bajdich, P. Chakthranont, C. Kirk, A. Vojvodic, T. F. Jaramillo, *Nat. Energy* **2016**, *1*, 16053.

[56] J. Suntivich, H. A. Gasteiger, N. Yabuuchi, H. Nakanishi, J. B. Goodenough, Y. Shao-Horn, *Nat. Chem.* **2011**, *3*, 546.

[57] D. A. Corrigan, R. M. Bendert, *J. Electrochem. Soc.* **1989**, *136*, 723.

[58] O. Diaz-Morales, I. Ledezma-Yanez, M. T. M. Koper, F. Calle-Vallejo, *ACS Catal.* **2015**, *5*, 5380.

[59] D. Friebel, M. W. Louie, M. Bajdich, K. E. Sanwald, Y. Cai, A. M. Wise, M.-J. Cheng, D. Sokaras, T.-C. Weng, R. Alonso-Mori, R. C. Davis, J. R. Bargar, J. K. Nørskov, A. Nilsson, A. T. Bell, *J. Am. Chem. Soc.* **2015**, *137*, 1305.

[60] M. S. Burke, M. G. Kast, L. Trotochaud, A. M. Smith, S. W. Boettcher, *J. Am. Chem. Soc.* **2015**, *137*, 3638.

[61] M. Gong, H. Dai, *Nano Res.* **2014**, *8*, 23.

[62] W. Chen, Y. Liu, Y. Li, J. Sun, Y. Qiu, C. Liu, G. Zhou, Y. Cui, *Nano Lett.* **2016**, *16*, 7588.

[63] L.-A. Stern, L. Feng, F. Song, X. Hu, *Energy Environ. Sci.* **2015**, *8*, 2347.

[64] K. Fan, H. Chen, Y. Ji, H. Huang, P. M. Claesson, Q. Daniel, B. Philippe, H. Rensmo, F. Li, Y. Luo, L. Sun, *Nat. Commun.* **2016**, *7*, 11981.

[65] X. Xu, F. Song, X. Hu, *Nat. Commun.* **2016**, *7*, 12324.

[66] A. Fujishima, K. Honda, *Nature* **1972**, *238*, 37.

[67] T. Hisatomi, J. Kubota, K. Domen, *Chem. Soc. Rev.* **2014**, *43*, 7520.

[68] R. Wang, A. Jayakumar, C. Xu, J. M. Lee, *ACS Sustain. Chem. Eng.* **2016**, *4*, 3736.

[69] Y. Li, J. Z. Zhang, *Laser Photonics Rev.* **2010**, *4*, 517.

[70] N. S. Lewis, *Nat. Nanotechnol.* **2016**, *11*, 1010.

[71] S. Hoang, P.-X. Gao, *Adv. Energy Mater.* **2016**, *6*, 1600683.

[72] A. Rabenau, *Angew. Chem. Int. Ed.* **1985**, *24*, 1026.

[73] U. Pal, P. Santiago, *J. Phys. Chem. B* **2005**, *109*, 15317.

[74] H. Wang, J. Xie, K. Yan, M. Duan, *J. Mater. Sci. Technol.* **2011**, *27*, 153.

[75] Q. Yang, Z. Lu, J. Liu, X. Lei, Z. Chang, L. Luo, X. Sun, *Prog. Nat. Sci. Mater. Int.* **2013**, *23*, 351.

[76] T. Adschiri, Y. Hakuta, K. Arai, *Ind. Eng. Chem. Res.* **2000**, *39*, 4901.

[77] G. Demazeau, *J. Mater. Sci.* **2008**, *43*, 2104.

[78] X. Ma, J. Liu, C. Liang, X. Gong, R. Che, *J. Mater. Chem. A* **2014**, *2*, 12692.

[79] W. Hao, S. Chen, Y. Cai, L. Zhang, Z. Li, S. Zhang, *J. Mater. Chem. A* **2014**, *2*, 13801.

[80] G. Xi, Y. Ye, Q. Ma, N. Su, H. Bai, C. Wang, *J. Am. Chem. Soc.* **2012**, *134*, 6508.

[81] L. Yu, H. Wu, T. Wu, C. Yuan, *RSC Adv.* **2013**, *3*, 23709.

[82] X. Liu, N. Zhang, R. Yi, G. Qiu, A. Yan, H. Wu, D. Meng, M. Tang, *Mater. Sci. Eng. B Solid-State Mater. Adv. Technol.* **2007**, *140*, 38.

[83] W. Feng, L. Chen, M. Qin, X. Zhou, Q. Zhang, Y. Miao, K. Qiu, Y. Zhang, C. He, *Sci. Rep.* **2015**, *5*, 17422.

[84] M. Gao, W. Sheng, Z. Zhuang, Q. Fang, S. Gu, J. Jiang, Y. Yan, *J. Am. Chem. Soc.* **2014**, *136*, 7077.

[85] H. Yang, Y. Zhang, F. Hu, Q. Wang, *Nano Lett.* **2015**, *15*, 7616.

[86] N. Parveen, M. H. Cho, *Sci. Rep.* **2016**, *6*, 27318.

[87] L. X. Yang, Y. J. Zhu, L. Li, L. Zhang, H. Tong, W. W. Wang, G. F. Cheng, J. F. Zhu, *Eur. J. Inorg. Chem.* **2006**, *23*, 4787.

[88] T. Yang, Y. Liu, Z. Huang, Q. Yang, M. Guan, M. Fang, X. Wu, *RSC Adv.* **2015**, *5*, 24486.

[89] H. Huang, W. Huang, Z. Yang, J. Huang, J. Lin, W. Liu, Y. Liu, *J. Mater. Chem. A* **2017**, *5*, 1558.

[90] Y. Yan, L. Thia, B. Y. Xia, X. Ge, Z. Liu, A. Fisher, X. Wang, *Adv. Sci.* **2015**, *2*, 1500120.

[91] X. Xia, C. Zhu, J. Luo, Z. Zeng, C. Guan, C. F. Ng, H. Zhang, H. J. Fan, *Small* **2014**, *10*, 766.

[92] B. J. Plowman, L. A. Jones, S. K. Bhargava, *Chem. Commun.* **2015**, *51*, 4331.

[93] D. Grujicic, B. Pesic, *Electrochim. Acta* **2002**, *47*, 2901.

[94] H. C. Shin, J. Dong, M. Liu, *Adv. Mater.* **2003**, *15*, 1610.

[95] H.-C. Shin, M. Liu, *Chem. Mater.* **2004**, *16*, 5460.

[96] S. Li, R. Furberg, M. S. Toprak, B. Palm, M. Muhammed, *Adv. Funct. Mater.* **2008**, *18*, 2215.

[97] N. D. Nikolić, K. I. Popov, L. J. Pavlović, M. G. Pavlović, *J. Electroanal. Chem.* **2006**, *588*, 88.

[98] H. Zhang, Y. Ye, R. Shen, C. Ru, Y. Hu, *J. Electrochem. Soc.* **2013**, *160*, 441.

[99] J. Suk, D. Y. Kim, D. W. Kim, Y. Kang, *J. Mater. Chem. A* **2014**, *2*, 2478.

[100] X. Yu, M. Wang, Z. Wang, X. Gong, Z. Guo, *Appl. Surf. Sci.* **2016**, *360*, 502.

[101] L. Vázquez-Gómez, E. Verlato, S. Cattarin, N. Comisso, P. Guerriero, M. Musiani, *Electrochim. Acta* **2011**, *56*, 2237.

[102] S. Cherevko, C. H. Chung, *Electrochim. Acta* **2010**, *55*, 6383.

[103] Y. Li, Y. Y. Song, C. Yang, X. H. Xia, *Electrochem. Commun.* **2007**, *9*, 981.

[104] D. K. Oppedisano, L. A. Jones, T. Junk, S. K. Bhargava, *J. Electrochem. Soc.* **2014**, *161*, D489.

[105] S. Cherevko, N. Kulyk, C.-H. Chung, *Nanoscale* **2012**, *4*, 103.

[106] C. Y. An, K. Zhuo, W. J. Kim, C. H. Chung, *Sensors Actuators, B Chem.* **2015**, *213*, 329.

[107] J. Yin, J. Jia, L. Zhu, *Int. J. Hydrogen Energy* **2008**, *33*, 7444.

[108] B. N. Choi, W. W. Chun, A. Qian, S. J. Lee, C. Chung, *Nanoscale* **2015**, *7*, 18561.

[109] Q. Wang, G. Wang, X. Han, X. Wang, J. G. Hou, *J. Phys. Chem. B* **2005**, *109*, 23326.

[110] R. Qiu, X. L. Zhang, R. Qiao, Y. Li, Y. Il Kim, Y. S. Kang, *Chem. Mater.* **2007**, *19*, 4174.

[111] I. Najdovski, P. Selvakannan, A. P. O'Mullane, *RSC Adv.* **2014**, *4*, 7207.

[112] L. Xiong, Y. X. Huang, X. W. Liu, G. P. Sheng, W. W. Li, H. Q. Yu, *Electrochim. Acta* **2013**, *89*, 24.

[113] M. G. Jeong, K. Zhuo, S. Cherevko, W. J. Kim, C. H. Chung, *J. Power Sources* **2013**, *244*, 806.

[114] S. Cherevko, N. Kulyk, C.-H. Chung, *Nanoscale* **2012**, *4*, 568.

[115] J. Liu, L. Cao, W. Huang, Z. Li, *J. Electroanal. Chem.* **2012**, *686*, 38.

[116] K.-H. Ye, Z.-Q. Liu, N. Li, K. Xiao, J. Wang, Y.-Z. Su, *J. Electrochem. Soc.* **2012**, *159*, D737.

[117] K. Zhuo, M. G. Jeong, C. H. Chung, *J. Power Sources* **2013**, *244*, 601.

[118] T. M. Silva, M. J. Carmezim, M. F. Montemor, *J. Phys. Chem. C* **2012**, *116*, 22425.

[119] C. González-Buch, I. Herraiz-Cardona, E. Ortega, J. García-Antón, V. Pérez-Herranz, *J. Appl. Electrochem.* **2016**, *46*, 791.

[120] X. Yu, M. Wang, Z. Wang, X. Gong, Z. Guo, *Electrochim. Acta* **2016**, *211*, 900.

[121] H. Liu, F. Ye, Q. Yao, H. Cao, J. Xie, J. Y. Lee, J. Yang, *Sci. Rep.* **2014**, *4*, 3969.

[122] P. Shahbazi, A. Kiani, *Electrochim. Acta* **2011**, *56*, 9520.

[123] S. Cherevko, N. Kulyk, C.-H. Chung, *Langmuir* **2012**, *28*, 3306.

[124] G. Zhang, S. Sun, M. Cai, Y. Zhang, R. Li, X. Sun, *Sci. Rep.* **2013**, *3*, 1526.

[125] J. B. Raoof, R. Ojani, A. Kiani, S. Rashid-Nadimi, *Int. J. Hydrogen Energy* **2010**, *35*, 452.

[126] A. Liu, H. Geng, C. Xu, H. Qiu, *Anal. Chim. Acta* **2011**, *703*, 172.

[127] H. T. Zhu, J. Luo, H. X. Yang, J. K. Liang, G. H. Rao, J. B. Li, Z. M. Du, *J. Phys. Chem. C* **2008**, *112*, 17089.

[128] C. Yuan, J. Li, L. Hou, X. Zhang, L. Shen, X. W. D. Lou, *Adv. Funct. Mater.* **2012**, *22*, 4592.

[129] X. Lu, X. Huang, S. Xie, T. Zhai, C. Wang, P. Zhang, M. Yu, W. Li, C. Liang, Y. Tong, *J. Mater. Chem.* **2012**, *22*, 13357.

[130] X. Xia, J. Tu, Y. Zhang, J. Chen, X. Wang, C. Gu, C. Guan, J. Luo, H. J. Fan, *Chem. Mater.* **2012**, *24*, 3793.

[131] Y.-M. Wang, X. Zhang, C.-Y. Guo, Y.-Q. Zhao, C.-L. Xu, H.-L. Li, *J. Mater. Chem. A* **2013**, *1*, 13290.

[132] K. Xu, R. Zou, W. Li, Q. Liu, X. Liu, L. An, J. Hu, *J. Mater. Chem. A* **2014**, 10090.

[133] J. Xing, S. Wu, K. Y. S. Ng, *RSC Adv.* **2015**, *5*, 88780.

[134] Q. Liu, J. Xu, Z. Chang, X. Zhang, *J. Mater. Chem. A* **2014**, *2*, 6081.

[135] X. Lu, C. Zhao, *Nat. Commun.* **2015**, *6*, 6616.

[136] Z. Li, M. Shao, H. An, Z. Wang, S. Xu, M. Wei, D. G. Evans, X. Duan, *Chem. Sci.* **2015**, *0*, 1.

[137] M. Wang, A. M. Anghel, B. Marsan, N.-L. Cevey Ha, N. Pootrakulchote, S. M. Zakeeruddin, M. Grätzel, *J. Am. Chem. Soc.* **2009**, *131*, 15976.

[138] K. S. Anuratha, S. Mohan, S. K. Panda, *New J. Chem.* **2016**, *40*, 1785.

[139] J.-Y. Lin, J.-H. Liao, T.-C. Wei, *Electrochem. Solid-State Lett.* **2011**, *14*, D41.

[140] H. Sun, D. Qin, S. Huang, X. Guo, D. Li, Y. Luo, Q. Meng, *Energy Environ. Sci.* **2011**, *4*, 2630.

[141] V. H. V. Quy, B.-K. Min, J.-H. Kim, H. Kim, J. A. Rajesh, K.-S. Ahn, *J. Electrochem. Soc.* **2016**, *163*, D175.

[142] J.-Y. Lin, J.-H. Liao, S.-W. Chou, *Electrochim. Acta* **2011**, *56*, 8818.

[143] J. Huo, J. Wu, M. Zheng, Y. Tu, Z. Lan, *Electrochim. Acta* **2015**, *180*, 574.

[144] W. Chen, C. Xia, H. N. Alshareef, *ACS Nano* **2014**, *8*, 9531.

[145] M. Yu, X. Li, Y. Ma, R. Liu, J. Liu, S. Li, *Appl. Surf. Sci.* **2017**, *396*, 1816.

[146] H. Khani, D. O. Wipf, *ACS Appl. Mater. Interfaces* **2017**, *9*, 6967.

[147] J. Liu, J. Wang, Z. Ku, H. Wang, S. Chen, L. Zhang, J. Lin, Z. X. Shen, *ACS Nano* **2016**, *10*, 1007.

[148] N. Jiang, L. Bogoev, M. Popova, S. Gul, J. Yano, Y. Sun, *J. Mater. Chem. A* **2014**, *2*, 19407.

[149] J. Wang, H. Zhong, Z. Wang, F. Meng, X. Zhang, *ACS Nano* **2016**, *10*, 2342.

[150] D. Bélanger, G. Laperriére, B. Marsan, *J. Electroanal. Chem.* **1993**, *347*, 165.

[151] D. Merki, S. Fierro, H. Vrubel, X. Hu, *Chem. Sci.* **2011**, *2*, 1262.

[152] J. L. Atwood, J. W. Steed, Eds., *Organic Nanostructures*, Wiley-VCH Verlag GmbH & Co. KGaA, Weinheim, Germany, **2008**.

[153] H.-C. "Joe" Zhou, S. Kitagawa, *Chem. Soc. Rev.* **2014**, *43*, 5415.

[154] K. Yamamoto, *Science* **2003**, *300*, 470.

[155] M. Eddaoudi, D. F. Sava, J. F. Eubank, K. Adil, V. Guillerm, *Chem. Soc. Rev.* **2015**, *44*, 228.

[156] K. Shen, X. Chen, J. Chen, Y. Li, *ACS Catal.* **2016**, *6*, 5887.

[157] W. Wang, X. Xu, W. Zhou, Z. Shao, *Adv. Sci.* **2017**, *4*, 1600371.

[158] X. Xiao, C.-T. He, S. Zhao, J. Li, W. Lin, Z. Yuan, Q. Zhang, S. Wang, L. Dai, D. Yu, *Energy Environ. Sci.* **2017**, *10*, 893.

[159] D. J. Tranchemontagne, J. L. Mendoza-Cortés, M. O'Keeffe, O. M. Yaghi, *Chem. Soc. Rev.* **2009**, *38*, 1257.

[160] D. J. Tranchemontagne, Z. Ni, M. O'Keeffe, O. M. Yaghi, *Angew. Chem. Int. Ed.* **2008**, *47*, 5136.

[161] Y. R. Lee, J. Kim, W. S. Ahn, *Korean J. Chem. Eng.* **2013**, *30*, 1667.

[162] Y. Sun, H.-C. Zhou, *Sci. Technol. Adv. Mater.* **2015**, *16*, 54202.

[163] A. J. Howarth, A. W. Peters, N. A. Vermeulen, T. C. Wang, J. T. Hupp, O. K. Farha, *Chem. Mater.* **2017**, *29*, 26.

[164] A. Banerjee, U. Singh, V. Aravindan, M. Srinivasan, S. Ogale, *Nano Energy* **2013**, *2*, 1158.

1700559 (24 of 25)

**ADVANCED
SCIENCE NEWS**

www.advancedsciencenews.com

**ADVANCED
ENERGY
MATERIALS**

www.advenergymat.de

[165] C. Li, T. Chen, W. Xu, X. Lou, L. Pan, Q. Chen, B. Hu, *J. Mater. Chem. A* **2015**, *3*, 5585.

[166] H. Guo, T. Li, W. Chen, L. Liu, J. Qiao, J. Zhang, *Sci. Rep.* **2015**, *5*, 13310.

[167] F. Zou, X. Hu, Z. Li, L. Qie, C. Hu, R. Zeng, Y. Jiang, Y. Huang, *Adv. Mater.* **2014**, *26*, 6622.

[168] K. S. Park, Z. Ni, A. P. Cote, J. Y. Choi, R. Huang, F. J. Uribe-Romo, H. K. Chae, M. O'Keeffe, O. M. Yaghi, *Proc. Natl. Acad. Sci.* **2006**, *103*, 10186.

[169] A. Phan, C. J. Doonan, F. J. Uribe-Romo, C. B. Knobler, M. O'Keeffe, O. M. Yaghi, *Acc Chem Res* **2010**, *43*, 58.

[170] C. Sun, J. Yang, X. Rui, W. Zhang, Q. Yan, P. Chen, F. Huo, W. Huang, X. Dong, *J. Mater. Chem. A* **2015**, *3*, 8483.

[171] Z. Jiang, Z. Li, Z. Qin, H. Sun, X. Jiao, D. Chen, *Nanoscale* **2013**, *5*, 11770.

[172] D. Yu, B. Wu, J. Ran, L. Ge, L. Wu, H. Wang, T. Xu, *J. Mater. Chem. A* **2016**, *4*, 16953.

[173] G. Zhan, H. C. Zeng, *Chem. Commun.* **2017**, *53*, 72.

[174] L. Han, X.-Y. Yu, X. W. (David) Lou, *Adv. Mater.* **2016**, *28*, 4601.

[175] X.-Y. Yu, L. Yu, H. Bin Wu, X. W. D. Lou, *Angew. Chem. Int. Ed.* **2015**, *54*, 5331.

[176] X.-Y. Yu, Y. Feng, Y. Jeon, B. Guan, X. W. D. Lou, U. Paik, *Adv. Mater.* **2016**, *28*, 9006.

[177] T. Y. Ma, S. Dai, M. Jaroniec, S. Z. Qiao, *J. Am. Chem. Soc.* **2014**, *136*, 13925.

[178] B. You, N. Jiang, M. Sheng, S. Gul, J. Yano, Y. Sun, *Chem. Mater.* **2015**, *27*, 7636.

[179] M. Liu, J. Li, *ACS Appl. Mater. Interfaces* **2016**, *8*, 2158.

[180] L. Jiao, Y.-X. Zhou, H.-L. Jiang, *Chem. Sci.* **2016**, *7*, 1690.

[181] J. Song, C. Zhu, B. Z. Xu, S. Fu, M. H. Engelhard, R. Ye, D. Du, S. P. Beckman, Y. Lin, *Adv. Energy Mater.* **2017**, *7*, 1601555.

[182] W. Zhou, J. Lu, K. Zhou, L. Yang, Y. Ke, Z. Tang, S. Chen, *Nano Energy* **2016**, *28*, 143.

[183] H. Bin Wu, B. Y. Xia, L. Yu, X.-Y. Yu, X. W. (David) Lou, *Nat. Commun.* **2015**, *6*, 6512.

[184] F.-X. Ma, H. Bin Wu, B. Y. Xia, C.-Y. Xu, X. W. D. Lou, *Angew. Chem.* **2015**, *127*, 15615.

[185] K. Sivula, R. van de Krol, *Nat. Rev. Mater.* **2016**, 15010.

[186] I. S. Cho, Z. Chen, A. J. Forman, D. R. Kim, P. M. Rao, T. F. Jaramillo, X. Zheng, *Nano Lett.* **2011**, *11*, 4978.

[187] Y. Qiu, K. Yan, H. Deng, S. Yang, *Nano Lett.* **2012**, *12*, 407.

[188] R. H. Coridan, K. a Arpin, B. S. Brunschwig, P. V. Braun, N. S. Lewis, *Nano Lett.* **2014**, *14*, 2310.

[189] P. Thiyagarajan, H. Ahn, J. Lee, J. Yoon, J.-H. Jang, *Small* **2013**, *9*, 2341.

[190] W. Wang, J. Dong, X. Ye, Y. Li, Y. Ma, L. Qi, *Small* **2016**, *12*, 1469.

[191] C. Liu, J. Tang, H. M. Chen, B. Liu, P. Yang, *Nano Lett.* **2013**, *13*, 2989.

[192] M. Li, R. Zhao, Y. Su, J. Hu, Z. Yang, Y. Zhang, *Adv. Mater. Interfaces* **2016**, *3*, 1600494.

[193] Z. Xu, M. Yin, J. Sun, G. Ding, L. Lu, P. Chang, X. Chen, D. Li, *Nanotechnology* **2016**, *27*, 115401.

[194] J. Low, J. Yu, M. Jaroniec, S. Wageh, A. A. Al-Ghamdi, *Adv. Mater.* **2017**, 1601694.

[195] H. Chen, Z. Wei, K. Yan, B. Yang, Z. Zhu, T. Zhang, S. Yang, *Small* **2014**, *10*, 4760.

[196] M. Fang, N. Han, F. Wang, Z. Yang, S. Yip, G. Dong, J. J. Hou, Y. Chueh, J. C. Ho, *J. Nanomater.* **2014**, *2014*, 1.

[197] M. Fang, H. Lin, H. Cheung, F. Xiu, L. Shen, S. Yip, E. Y.-B. Pun, C.-Y. Wong, J. C. Ho, *ACS Appl. Mater. Interfaces* **2014**, *6*, 20837.

[198] P. M. Rao, L. Cai, C. Liu, I. S. Cho, C. H. Lee, J. M. Weisse, P. Yang, X. Zheng, *Nano Lett.* **2014**, *14*, 1099.

[199] S. A. Maier, *Plasmonics: Fundamentals and Applications*, Springer US, Boston, MA, **2007**.

[200] C. M. Hsu, C. Battaglia, C. Pahud, Z. Ruan, F. J. Haug, S. Fan, C. Ballif, Y. Cui, *Adv. Energy Mater.* **2012**, *2*, 628.

[201] S. Y. Chou, W. Ding, *Opt. Express* **2013**, *21 Suppl 1*, A60.

[202] D. H. Lee, J. Y. Kwon, S. Maldonado, A. Tuteja, A. Boukai, *Nano Lett.* **2014**, *14*, 1961.

[203] M. M. Adachi, A. J. Labelle, S. M. Thon, X. Lan, S. Hoogland, E. H. Sargent, *Sci. Rep.* **2013**, *3*, 2928.

[204] S. K. Cushing, N. Wu, *J. Phys. Chem. Lett.* **2016**, *7*, 666.

[205] G. Kakavelakis, I. Vangelidis, A. Heuer-Jungemann, A. G. Kanaras, E. Lidorikis, E. Stratakis, E. Kymakis, *Adv. Energy Mater.* **2016**, *6*, 1.

[206] Y. H. Jang, Y. J. Jang, S. Kim, L. N. Quan, K. Chung, D. H. Kim, *Chem. Rev.* **2016**, *116*, 14982.

[207] S. Carretero-Palacios, A. Jiménez-Solano, H. Míguez, *ACS Energy Lett.* **2016**, *1*, 323.

[208] W. R. Erwin, H. F. Zarick, E. M. Talbert, R. Bardhan, *Energy Environ. Sci.* **2016**, *9*, 1577.

[209] Y. H. Lee, T. K. Lee, I. Song, H. Yu, J. Lee, H. Ko, S. K. Kwak, J. H. Oh, *Adv. Mater.* **2016**, *28*, 4976.

[210] C. Jia, X. Li, N. Xin, Y. Gong, J. Guan, L. Meng, S. Meng, X. Guo, *Adv. Energy Mater.* **2016**, *6*, 1600431.

[211] K. L. Kelly, E. Coronado, L. L. Zhao, G. C. Schatz, *J. Phys. Chem. B* **2003**, *107*, 668.

[212] E. Hutter, J. H. Fendler, *Adv. Mater.* **2004**, *16*, 1685.

[213] J. Li, S. K. Cushing, P. Zheng, F. Meng, D. Chu, N. Wu, *Nat. Commun.* **2013**, *4*, 2651.

[214] F. Ning, M. Shao, S. Xu, Y. Fu, R. Zhang, M. Wei, D. G. Evans, X. Duan, *Energy Environ. Sci.* **2016**, *9*, 2633.